Diversity and evolution of a phase-variable multi-locus antigen in *Neisseria gonorrhoeae*

QinQin Yu[1,2], Tatum D. Mortimer[3], Sofia O.P. Blomqvist[1,2], Bailey Bowcutt[1,2], David Helekal[1,2], Samantha G. Palace[1,2], Yonatan H. Grad[1,2]*

[1] Department of Immunology and Infectious Diseases, Harvard T. H. Chan School of Public Health, Boston, Massachusetts, United States of America

[2] Center for Communicable Disease Dynamics, Harvard T. H. Chan School of Public Health, Boston, Massachusetts, United States of America

[3] Department of Population Health, University of Georgia College of Veterinary Medicine, Athens, Georgia, United States of America

* Corresponding author

Email: ygrad@hpsh.harvard.edu

Short title: Antigenic variation in *Neisseria gonorrhoeae*

Abstract

Neisseria gonorrhoeae is a sexually transmitted bacterial pathogen that deploys multiple mechanisms to evade the immune system, including rapid variation in surface antigens. One of the most abundant and diverse antigens is the Opacity (Opa) protein, a surface protein that mediates gonococcal attachment to host receptors. Studies of Opa diversity and evolution have been limited by the inability of short-read sequencing to resolve the multiple copies of *opa* in each genome, preventing a comprehensive understanding of antigenic variation for vaccine design and immunology studies. We assembled a dataset of 219 complete genomes from diverse clinical isolates using long-read sequencing and developed bioinformatics and phylogenetics tools to assess *opa* variation quantitatively. Each genome had on average 7 distinct *opa* alleles at 9 to 12 *opa* loci, and almost all isolates had at least one pair of identical or near-identical *opa* genes. Fewer *opa* genes were in frame, and thus inferred to be expressed, than expected due to chance. While genomic distance between isolates correlated with overall *opa* allele sequence similarity, *opa* genes were on average 74 times more diverse than the rest of the genome. One *opa* locus evolved more rapidly than the other loci. There was little evidence that interspecies recombination contributed to *N. gonorrhoeae opa* diversity. Our findings reveal a continuously evolving *opa* repertoire that leads to diverse *opa* alleles even in closely related strains and indicate that there are likely unknown biological factors modulating *opa* expression.

Author Summary

The rising levels of antibiotic resistance in *Neisseria gonorrhoeae* make controlling the spread of this sexually transmitted pathogen a public health priority. *N. gonorrhoeae* rapidly varies surface proteins to evade recognition by the human adaptive immune system. Understanding how these proteins evolve may help us design better vaccines and control measures for curbing the spread

of gonorrhea. One of the most abundant surface proteins is the Opacity protein (Opa), which helps *N. gonorrhoeae* bind to host cells upon colonization. Research efforts to understand the evolution of Opa have been limited because it is encoded by multiple genes in the genome that are not resolved by short-read sequencing technologies. Here, we resolved the genes that encode Opa using a dataset of 132 publicly available complete genomes and 87 genomes that we completed using long-read sequencing of diverse clinical isolates. We found that Opa evolves rapidly to generate different versions of the protein in the same isolate, but very few of these protein versions appear expressed. We also found evidence that there may be other, uncharacterized mechanisms that control how these proteins evolve over longer timescales.

Introduction

In 2020, the World Health Organization (WHO) estimated there were more than 82 million cases worldwide of gonorrhea, the sexually transmitted infection caused by the obligate human pathogen *Neisseria gonorrhoeae*. Gonorrhea is a WHO priority pathogen due to increasing levels of antibiotic resistance and no highly-effective vaccine [1]. Infection does not appear to confer protection, such that individuals can be reinfected [2], even by the same strain [3], reflecting *N. gonorrhoeae*'s escape from the host immune system [4,5].

One of the ways *N. gonorrhoeae* achieves this immune evasion is through rapidly varying its antigens [6,7]. A major surface protein that undergoes this variation is the Opacity protein (Opa) [8–11]. Opa proteins mediate gonococcal attachment to host receptors during colonization [12–17] and may be involved in suppression of the host immune response, though the mechanisms are as yet unclear [15,18]. These proteins are encoded by multiple highly diverse *opa* genes in separate loci in each *N. gonorrhoeae* genome [10,19]. A series of pentanucleotide repeats in the 5' end of the coding sequence determines whether each of these genes is in frame and fully

translated, and changes in the repeat copy number, likely from slip-strand repair, result in phase variation [20].

Studies of *opa* variation and evolution have focused on small numbers of isolates or closely related isolates [9,19,21]. These studies showed that *opa* genes have high sequence diversity within and between isolates [9], recombination within isolates plays a key role in generating new sequence diversity [11,21], and gene conversion events can lead to two identical or near-identical *opa* alleles [20–22]. Bilek et al. [21] observed that one *opa* gene varied more in closely related isolates than the other *opa* loci. There is also evidence that *opa* loss occasionally occurs [21] and few *opa* are phase on in each isolate [20]. Phylogenetic analysis of *opa* from *N. gonorrhoeae, N. meningitidis,* and the commensals *N. flava* and *N. sicca* showed that *opa* clustered by species [9].

However, due to the small numbers of isolates in these studies, we lack generalizable quantitative patterns and thus have a limited understanding of *N. gonorrhoeae opa* sequence variation and evolution. Several obstacles have prevented studies of *opa* diversity in larger numbers of isolates. Polymerase chain reaction can amplify the *opa* regions [19,21], but this approach is challenging to scale up due to unknown primer coverage of the *opa* repertoire. *opa* sequences cannot be resolved using short-read whole-genome sequencing platforms, such as Illumina, as the multiple and highly similar *opa* loci are problematic for mapping and genome assembly. Furthermore, the high diversity of *opa* has made it challenging to analyze sequences using standard bioinformatics, phylogenetics, and phylodynamic approaches, in that methods are designed primarily for single copy genes.

Long-read sequencing enables us to overcome these challenges. We combined publicly available complete genomes with diverse genomes that we sequenced using the Oxford

95 Nanopore long-read platform. We developed bioinformatic and phylogenetic approaches for
96 defining the diversity and evolution of highly variable multilocus antigens and applied them to
97 the largest set of *opa* sequences to date to investigate *opa* variation. Finally, we developed a
98 sequence-based clustering approach for *opa* alleles in the effort towards establishing a
99 standardized nomenclature to facilitate comparison of *opa* alleles in future studies.
100
101 **Methods**
102
103 Dataset of high-quality complete genomes
104
105 *Publicly available complete genomes*
106 We searched for "*Neisseria gonorrhoeae*" in the National Center for Biotechnology Information
107 Genome Datasets (https://www.ncbi.nlm.nih.gov/datasets/genome/) and downloaded all
108 genomes with an assembly level of "chromosome" or "complete" on July 31, 2025. We
109 determined the sequencing technology and assembly method from the associated publications
110 (where available) and associated metadata available on NCBI. In the rare cases of
111 discrepancies between the publication and NCBI, we used the metadata reported in the
112 publication.
113
114 *Nanopore sequencing and genome assembly*
115 *N. gonorrhoeae* isolates were streaked from frozen stocks onto GCB agar (Difco) with Kellogg's
116 supplement [23] and grown at 37° C with 5% CO_2 overnight. Genomic DNA was extracted using
117 the Invitrogen PureLink Genomic DNA Mini Kit. We prepared the library using the Oxford
118 Nanopore Native Barcoding Kit 24 V14 (SQK-NBD114.24) and performed Nanopore
119 sequencing using a MinION Mk1B device. Basecalling was performed using Dorado v0.8.2 [24]
120 superaccuracy basecalling. Reads were demultiplexed using Dorado v0.8.2 demux and filtered

121 using Filtlong v0.2.1 (https://github.com/rrwick/Filtlong) to keep the 90% highest quality read
122 bases and only reads longer than 1kbp. Genomes were assembled using Autocycler v0.2.1 [25]
123 with 4 read subsets at 25x minimum depth and using the assemblers: Canu v2.2 [26], Flye
124 v2.9.5 [27], miniasm v0.3 [28], NECAT v0.0.1 [29], NextDenovo v2.5.2 [30], and Raven v1.8.3
125 [31]. Genomes that were fully resolved (one complete genome plus optional plasmids) and had
126 a length of at least 2 Mbp were kept, as we expect the length of the *N. gonorrhoeae* genome to
127 be 2.2 Mbp.
128
129 Identifying *opa* genes in complete genomes
130
131 Genomes were rotated using the rotate program v1.0 [32] to match the first 90 bases of *dnaA*
132 from FA1090 (NC_002946.2), allowing for up to 5 mismatches. We wrote a custom script to
133 identify *opa* genes that searched for the tandem pentanucleotide repeats (CTCTT) and a unique
134 conserved sequence near the stop codon [19,21]. Details of the algorithm are presented in the
135 Supplementary Information. The N-terminus of the mature protein was found by searching for
136 the sequence GCAAGTGA [20], allowing at most 2 substitutions. Only sequences that have an
137 identified start codon, stop codon, and N-terminus are determined to be intact *opa* genes. Intact
138 *opa* genes were given a number starting from 1 in the order that they appeared in the rotated
139 genome (i.e., FA1090 *opa1* is the first *opa* in FA1090 after *dnaA*). The *opa* sequence was
140 determined to be in frame if the number of nucleotides between the start codon and the N-
141 terminus was a multiple of 3.
142
143 *Comparison to other sequence search methods*
144 To confirm that we had identified all the *opa* genes in the genomes, we compared our method to
145 three additional approaches:
146

147 1. We performed a search of the conserved region of the FA1090 *opa1* sequence between
148 the semivariable and hypervariable 1 regions using BLAST v2.14.1. We set the
149 maximum number of high-scoring segment pairs (local alignments) to keep as 15 for a
150 single query-subject pair and kept all other parameters at the default values. We
151 matched the hits from the BLAST results that were also found by our search algorithm
152 by merging the nearest start positions of the hits from the two search algorithms if they
153 were within 1200 nucleotides. BLAST hits that were not merged were identified as
154 putative additional hits found by BLAST not found by our search algorithm and we
155 manually inspected these sequences.
156 2. We annotated the genomes using Prokka v1.14.6 [33]. We set the genus to "Neisseria"
157 and species to "gonorrhoeae" and kept all other parameters at their default values. We
158 noticed that all the *opa* genes identified with our method had the gene name *piiC_**,
159 where * was a number. We then checked if there were any additional genes annotated
160 as *piiC_** that were not identified by our method.
161 3. We used Roary v3.13.0 [34] to define the pan-genome and cluster genes. We set the
162 minimum percentage identity for the BLASTp program within Roary to be 90% and kept
163 all other parameters at their default values. We looked at gene clusters that included the
164 *opa* genes identified by our method to assess for additional genes in those clusters not
165 identified by our method.
166

167 *Identification of truncated* opa

168 To identify truncated *opa* that were missing the start and/or stop codon, we extracted the
169 sequences, including upstream and downstream sequences, of the hits found by BLAST that
170 were not found by our search algorithm and aligned the sequences with the FA1090 *opa*
171 sequences using MAFFT v7.520 [35]. We visualized the alignments using JalView v2.11.5.1
172 [36] to identify if each hit was a truncated *opa* compared to the FA1090 *opa* sequences.

173

174 *Genomic rearrangements*

175 Genomic rearrangements were detected using progressiveMauve v2.4.0 [37] by comparing
176 each complete genome (query) with the complete FA1090 genome (reference). We rearranged
177 the *opa* position in the query genome relative to the reference genome by reordering and
178 flipping regions of the query genome that fell into locally collinear blocks compared to the
179 reference. Regions of the query genome that did not fall into any locally collinear block with the
180 reference genome were not altered.

181

182 Whole genome phylogenies

183

184 *Generating reference-mapped pseudogenomes*

185 To generate reference-mapped pseudogenomes, we used short reads generated by, or
186 simulated to be generated by, Illumina sequencing. Sequencing reads from all publicly available
187 *N. gonorrhoeae* datasets were downloaded from the European Nucleotide Archive (**Table S3**
188 and https://github.com/qinqin-
189 yu/gonococcus_opa_diversity/blob/main/opa_diversity_snakemake/input_data/whole_genome_
190 metadata/global_isolates_metadata_met_qc.csv). For the publicly available complete genomes,
191 we used ART v2016.06.05 [38] to simulate paired-end short reads from the MiSeq v3
192 sequencing system with a read length of 250 bp, 80x coverage, mean DNA fragment size of 600
193 and standard deviation of 100. Reads were mapped to the NCCP11945 (NC_011035.1)
194 reference genome using BWA-MEM v0.7.17 [39]. Duplicate reads were marked with Picard
195 v3.0.0 (https://broadinstitute.github.io/picard/), and reads were sorted with SAMtools v1.17 [40].
196 The quality of the mapped reads was assessed using Qualimap's bamqc v2.2.1 [41]. We used
197 Pilon v1.24 [42] to call variants (minimum mapping quality 20 and minimum coverage of 10). To
198 create pseudogenomes, we replaced the reference allele with high quality variant calls (at least

199 90% of reads supporting the allele). Positions called as deletions by Pilon were replaced with a
200 gap character, and positions with low coverage or an indeterminate allele were replaced with an
201 N.
202
203 *Selecting representative global genomes*
204 To select representative global genomes from the publicly available *N. gonorrhoeae* isolates,
205 we included isolates with genomes meeting the following quality control filters: at least 80% of
206 reads mapped to the *N. gonorrhoeae* reference genome, the coverage of reads mapped to the
207 *N. gonorrhoeae* reference genome was >40X, fewer than 12% of the sites in the *N.*
208 *gonorrhoeae* reference genome were unable to be confidently called using our assembly
209 pipeline, and the *de novo* assembly length was 1.75 Mbp-2.5 Mbp. This yielded 21,653
210 genomes which were then clustered using PopPUNK v2.6.0 [43]. The isolate in each PopPUNK
211 cluster with the fewest contigs in its *de novo* assembly was chosen as the representative isolate
212 from that cluster, resulting in 737 representative genomes (**Table S4**).
213
214 *Recombination-masked phylogenies*
215 Recombination-masked phylogenetic trees were created using the reference-mapped
216 pseudogenomes in Gubbins v3.3.4 [44] using the GTR substitution model, the RAxML Next
217 Generation tree builder [45], a maximum of 20 iterations for the phylogeny of complete
218 genomes, and a maximum of 5 iterations for the phylogeny of representative and complete
219 genomes.
220
221 <u>Quantifying *opa* diversity</u>
222
223 *Comparison of within- and between-isolate opa diversity*

224 To compare within- and between-isolate *opa* diversity, we first translated the *opa* sequences
225 downstream of the coding repeats. We excluded all sequences with premature stop codons due
226 to frameshift mutations downstream of the coding repeats or nonsense mutations. We then
227 aligned the amino acid sequences using MAFFT v7.520 [35] with the default parameters. We
228 then calculated pairwise distances in the alignment for all pairs of *opa* sequences from different
229 isolates (between-isolate comparison) and all pairs of *opa* sequences from the same isolate
230 (within-isolate comparison).
231
232 *Similar* opa *within the same isolate*
233 To identify clusters of similar *opa* sequences from the same strain, we used the NetworkX
234 Python package (https://github.com/networkx/networkx) to create graphs where the nodes are
235 the *opa* sequences and the edges connect *opa* sequences with less than 5% difference in
236 amino acid sequence alignment. The clusters of similar *opa* sequences were identified as the
237 connected components in the graph. The percentage of isolates with at least one pair of similar
238 *opa* was determined by finding the isolates that contained at least one *opa* sequence with less
239 than 5% difference in amino acid sequence alignment with another *opa* sequence in the same
240 strain.
241
242 *Comparison of* opa *sequence distance and genomic sequence distance*
243 We calculated the *opa* sequence distance and the genomic distance between pairs of genomes.
244 To facilitate quantitative comparisons between pairs of genomes, only pairs of genomes with the
245 same number of *opa* genes were kept. The *opa* sequence distance was calculated using the
246 alignment generated above and pairing the *opa* sequences between the two genomes that had
247 the fewest number of segregating sites using a greedy algorithm (i.e., find the two closest *opa*
248 sequences, then find two next closest *opa* sequences, etc. If there are identical matches, then
249 one is chosen at random to be matched.). The total *opa* sequence distance was calculated by

250 summing the distances between each pair of *opa* sequences and dividing by the number of *opa*
251 genes (where a distance of 0 indicates the *opa* repertoire in the two genomes are identical and
252 a distance of 1 indicates that all sites in all *opa* genes in the two genomes are different).
253
254 The pairwise genomic sequence distance was calculated as the number of SNPs between pairs
255 of pseudogenomes divided by the length of the pseudogenome using pairsnp v0.3.1
256 (https://github.com/gtonkinhill/pairsnp). Missing sites (indicated by N) were excluded in the
257 calculation of the SNP distance. Sites that were missing in some isolates but present in the two
258 isolates being compared were included.
259
260 *Other* Neisseria *species* opa
261 *Identifying* opa *genes*
262 We downloaded complete genomes ("chromosome" or "complete" assembly levels) from NCBI
263 RefSeq on February 13, 2025 using the search term "Neisseria" and filtered out all *N.*
264 *gonorrhoeae* genomes (**Table S5**). Genomes were rotated using the rotate program v1.0 [32] to
265 match the first 90 bases of *dnaA* from FA1090 (NC_002946.2), allowing for up to 5 mismatches.
266 If this sequence was not found, then the unrotated genome was used for downstream analysis.
267 This occurred in 60/198 (30%) genomes. We identified *opa* genes using the custom script that
268 we used for *N. gonorrhoeae*, which looks for the coding repeats and the unique conserved
269 sequence near the stop codon. To look for additional *opa* that were missed by our script, we
270 BLASTed the conserved regions of *N. gonorrhoeae* FA1090 *opa1*.
271
272 *Assessing sequence relatedness*
273 We calculated the k-mer distances using MASH v2.3 [46] with a k-mer size of 9 and used the
274 distances as input to create a neighbor joining tree using rapidNJ v2.3.2 [47].
275

276 Clustering of variable region sequences

277

278 *Definition of semivariable, hypervariable 1, and hypervariable 2 region sequences*

279 We aligned the nucleotide sequences of all *opa* genes using MAFFT v7.520 [35] with a gap
280 opening penalty of 4 and a gap extension penalty of 1. The nucleotide sequence of FA1090
281 *opa1* was compared to the sequences in Bhat et al. [19] to identify the semivariable,
282 hypervariable 1, and hypervariable 2 region sequences. The variable regions in the other *opa*
283 sequences were determined based on where they aligned to FA1090 *opa1*.

284

285 *Calculation of k-mer distance*

286 The k-mer distances between sequences in each of the semivariable, hypervariable 1, and
287 hypervariable 2 regions were calculated using MASH v2.3 [46] with a k-mer size of 6 for the
288 semivariable region and 7 for the hypervariable 1 and hypervariable 2 regions. These k-mer
289 sizes were chosen so that the probability of observing a random sequence of length k in a
290 random sequence the length of each region was 0.01. The p-value is the probability of
291 observing a given k-mer distance (or less) under the null hypothesis that both sequences are
292 random collections of k-mers.

293

294 *Clustering*

295 The variable region sequences were clustered using the Markov Cluster Algorithm (MCL)
296 v14.137 [48]. We constructed a distance matrix using the -log10 transformed p-value from
297 MASH and values larger than 200 were set to 200. We made these transformations following
298 the approach in TRIBE-MCL, which clusters proteins using -log10 transformed e-values from
299 BLAST [49]. The distance matrix was input into MCL, which then performs multiple rounds of
300 expansion and contraction to amplify large values and reduce small values of the matrix. The
301 number of rounds of expansion and contraction is set by the inflation parameter. We ran the

clustering using a range of inflation parameters: 1.4, 2, 4, 6, 8, 10, 12, and 14. We chose the inflation parameter that gave a stable clustering, inspired by TRIBE-MCL. A stable clustering was defined as having a percentage difference in clustering with the next lowest inflation parameter as less than 1% for the semivariable and hypervariable 2 regions. For the hypervariable 1 region, we relaxed the definition for a stable clustering as having less than a 5% difference in clustering with the next lowest inflation parameter due to the large number of clusters. The percentage difference in clustering is calculated as the sum of the number of nodes (sequences) that must be exchanged to transform the two clusterings into each other (also called the split/join distance) divided by two times the number of sequences. The motivation for this approach is that TRIBE-MCL uses convergence of outputs to determine the inflation parameter.

The cluster sequence logos were visualized by aligning the nucleotide sequences in each cluster using MAFFT v7.520 [35] with the default parameters and plotting the sequence logos with Logomaker v0.8 [50].

<u>Ancestral state reconstruction</u>

Dated phylogeny

Pseudogenomes were generated as described above but with the reference genome being one randomly selected genome from the subtree. Regions of the genome under recombination were detected using Gubbins v3.3.4 [44] (GTR substitution model, RAxML Next Gen tree builder, 20 iterations) and masked. The recombination-masked alignment was used to build a dated phylogeny in BEAST2 v2.7.5 [51], for all isolates that had date of collection information. When the date was given as a year, we set the date to January 1 of that year. We used a GTR

328 substitution model with gamma rate heterogeneity (4 categories), a strict clock model, a
329 coalescent constant population, and 100,000,000 chain length. Chains were inspected to
330 confirm good mixing (effective sample size greater than 200).
331
332 *Ancestral state reconstruction*
333
334 We performed ancestral state reconstruction for each of the loci and variable region cluster
335 types separately on the dated phylogeny using PastML v1.9.49 [52] with the default parameters.
336 Isolates that did not have an intact *opa* at a locus were not included for the inference at that
337 locus. If there were no changes to the variable region cluster type at a locus then the average
338 rate of cluster type changes was set to 0.
339
340 Phylogenies
341 Mutation-scaled phylogenies were visualized in iTOL v6.9.1 [53] using midpoint rooting. The
342 time-scaled phylogeny was visualized in FigTree v1.4.4
343 (http://tree.bio.ed.ac.uk/software/figtree/).
344
345 Statistical analyses
346 Statistical analyses and plotting were done in Python v3.13.1.
347
348 Data availability
349 The Nanopore sequencing reads and assembled complete genomes generated in this study are
350 available at the European Nucleotide Archive under study accession PRJEB106623:
351 http://www.ebi.ac.uk/ena/browser/view/PRJEB106623.
352
353 Code availability

354 Our code for performing the analyses has been compiled into a Snakemake [54] pipeline for
355 reproducibility. The code is available in GitHub (https://github.com/qinqin-
356 yu/gonococcus_opa_diversity).
357
358 **Results**
359
360 A diverse set of 219 complete genomes of *N. gonorrhoeae*
361
362 Because long-read only assemblies using older sequencing technologies have a higher error
363 rate, we filtered the publicly available complete genome assemblies to include only those
364 assembled using long-read and short-read data, which yielded 132 complete genomes (**Table**
365 **S1**). To complement the publicly available complete genomes of *N. gonorrhoeae*, we
366 sequenced an additional 87 isolates from across the *N. gonorrhoeae* phylogeny using Oxford
367 Nanopore long-read sequencing (**Figure 1, Table S2**). In total, this gave 219 complete
368 genomes.
369
370 Comparison of three long-read only assembly methods (see Supplementary Methods) on two
371 isolates whose genomes differed by 6648 SNPs showed that Autocycler performed the best,
372 with no changes to the *opa* sequences for read depths of 21-140x (**Figure S 1** and
373 Supplementary Information). Polishing the Autocycler assemblies with short-read data did not
374 change the *opa* sequences at any read depth, showing that the long-read data was sufficient to
375 reconstruct the *opa* sequences. Further testing on a larger set of 11 diverse isolates indicated
376 that varying read depths resulted in differences in *opa* sequence for only 4 out of 119 *opa*
377 sequences in long-read only assemblies with Autocycler (3 SNPs and one *opa* that was
378 undetected or had large numbers of sequence differences; see **Figure S 2** and Supplementary
379 Information).

380

381 Identification of *opa* genes

382

383 Across the 219 complete genomes, we identified 2,359 full length *opa* genes. To determine if
384 we missed any *opa* sequences, we compared our approach to three standard strategies to
385 identify homologous genes: BLAST, Prokka, and pangenome clustering of the Prokka
386 annotations. Using BLAST to search for the conserved region of the *opa* gene did not identify
387 any additional intact *opa* genes compared to our method, but it did identify 35 additional
388 truncated *opa* genes and 2 *opa* genes with a mutation in the start codon (ACG instead of ATG).
389 Our method identified 8 *opa* genes not found by BLAST that were divergent from other *opa*
390 sequences. Gene annotations using Prokka identified the same 37 truncated *opa* genes or *opa*
391 genes with a mutation in the start codon found by the BLAST search, but no additional genes.
392 Our method identified 2 additional *opa* genes that were not annotated by Prokka. Pangenome
393 clustering identified the 37 truncated *opa* genes or *opa* genes with a mutation in the start codon
394 found by the BLAST search and one additional truncated *opa*. Our method identified 7 *opa*
395 genes not found in the pangenome clusters, including the 2 *opa* genes that were not annotated
396 by Prokka. In summary, our method of searching for *opa* genes identified the most
397 comprehensive set of *opa* genes from the genomes and, to our knowledge, did not miss any
398 intact *opa* genes.

399

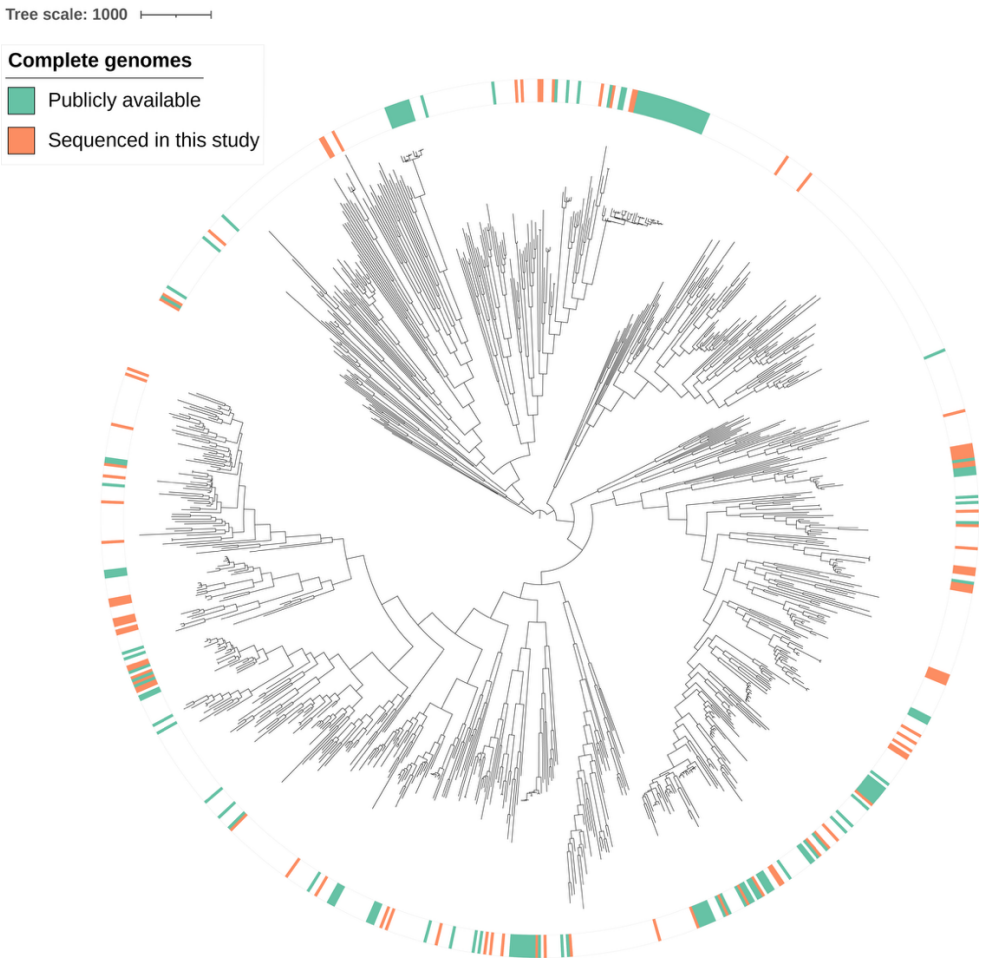

Figure 1: **A diverse set of *N. gonorrhoeae* complete genomes.** Recombination-masked phylogeny of the publicly available complete genomes (generated with long- and short-read sequencing data, green) and the new complete genomes generated in this study (generated with Oxford Nanopore sequencing, orange), in the context of a representative global collection of *N. gonorrhoeae* isolates (generated with short-read sequencing data). The tree scale indicates the number of recombination-masked SNPs.

<u>Consistent local genomic positioning of *opa* reveals patterns of copy number variation</u>

411 We next determined the number and locations of *opa* genes in each genome. Out of 219
412 genomes, 5 genomes (2.3%) had 9 *opa* genes, 41 genomes (18.7%) had 10 *opa* genes, 172
413 genomes (78.5%) had 11 *opa* genes, and 1 genome (0.5%) had 12 *opa* genes. The genome
414 with 12 *opa* genes (WHO_T_2024) contained a duplication of 47,339 nucleotides with 2 SNPs
415 that led to the exact duplication of one of the *opa* genes. Based on the genomes in this study,
416 we observed *opa* losses a handful of times across the phylogeny (**Figure 2a**). In addition, there
417 were 35 sequences that contained part of an *opa* gene. Of these, 28 occurred in a
418 phylogenetically related cluster of isolates and were missing the last 260 nucleotides of the
419 gene, including the hypervariable 2 region, in the context of an approximately 400 nucleotide
420 deletion that also included 140 nucleotides of sequence downstream of the *opa* gene. These 28
421 clustered, truncated *opa* sequences were similar but not identical and occurred in similar
422 locations in the genome. There were also 2 sequences with a mutation in the start codon (ACG
423 instead of ATG) that otherwise were full length *opa* genes. All but one of the truncated *opa*
424 sequences and both *opa* sequences with a mutation in the start codon occurred in genomes
425 that had fewer than 11 intact and full length *opa* genes. If all genomes were to have at least 11
426 *opa*, then there would be at least 51 missing full length *opa* across the dataset, 37 of which are
427 accounted for here.
428
429 The genomic locations of *opa* genes were variable across genomes (**Figure S 3**), with a mean
430 distance of 59,460 nucleotides between *opa* gene loci across strains. We observed that the
431 pattern of genomic organization of *opa* loci clustered phylogenetically (**Figure 2a)**. To test
432 whether differences in *opa* locations were due to large-scale genomic rearrangements, we used
433 alignments to the reference strain FA1090 to detect and then correct for such rearrangements
434 (**Figure S 4**). We found 2,331/2,359 (98.8%) *opa* genes within locally collinear alignment blocks
435 with the FA1090 genome. The mean distance between *opa* locations in the rearrangement-
436 corrected assemblies decreased to 2,886 nucleotides (**Figure 2a, Figure S 3**). The consistency

437 of *opa* locations in the rearrangement-corrected assemblies allowed us to define 11 loci, which
438 we named in the order that they appeared in FA1090 from *opaA* to *opaK* (**Figure 2b**). Loss of
439 full-length *opa* genes occurred most often in *opaB* (16% of all isolates), *opaK* (9% of all
440 isolates), and *opaI* (5% of all isolates) (**Figure 2c**). There were 15/2,359 (0.6%) *opa* that did not
441 fall within these 11 loci.
442
443 Of the 2,359 *opa* genes, 156 (6.6%) had a frameshift mutation after the end of the coding repeat
444 sequence, leading to a stable premature stop codon independent of phase variation. This
445 included at least one *opa* gene in 51/132 (39%) of publicly available genomes and 29/87 (33%)
446 genomes sequenced in this study. None of the superseded WHO reference strains [55] had
447 these frameshift mutations. For the genomes sequenced in this study, there was a negative
448 correlation between the sequencing coverage and the number of *opa* with these frameshift
449 mutations (**Figure S 5a**, Spearman correlation coefficient -0.45, $p=10^{-5}$), suggesting that some
450 of these frameshift mutations may be due to sequencing error. The premature stop codons were
451 concentrated in three locations in the *opa* gene (**Figure S 5b**) and closer inspection of the
452 nucleotide sequences revealed that variations in the semivariable region sequence upstream of
453 the premature stop codon led to the frameshift mutations.
454

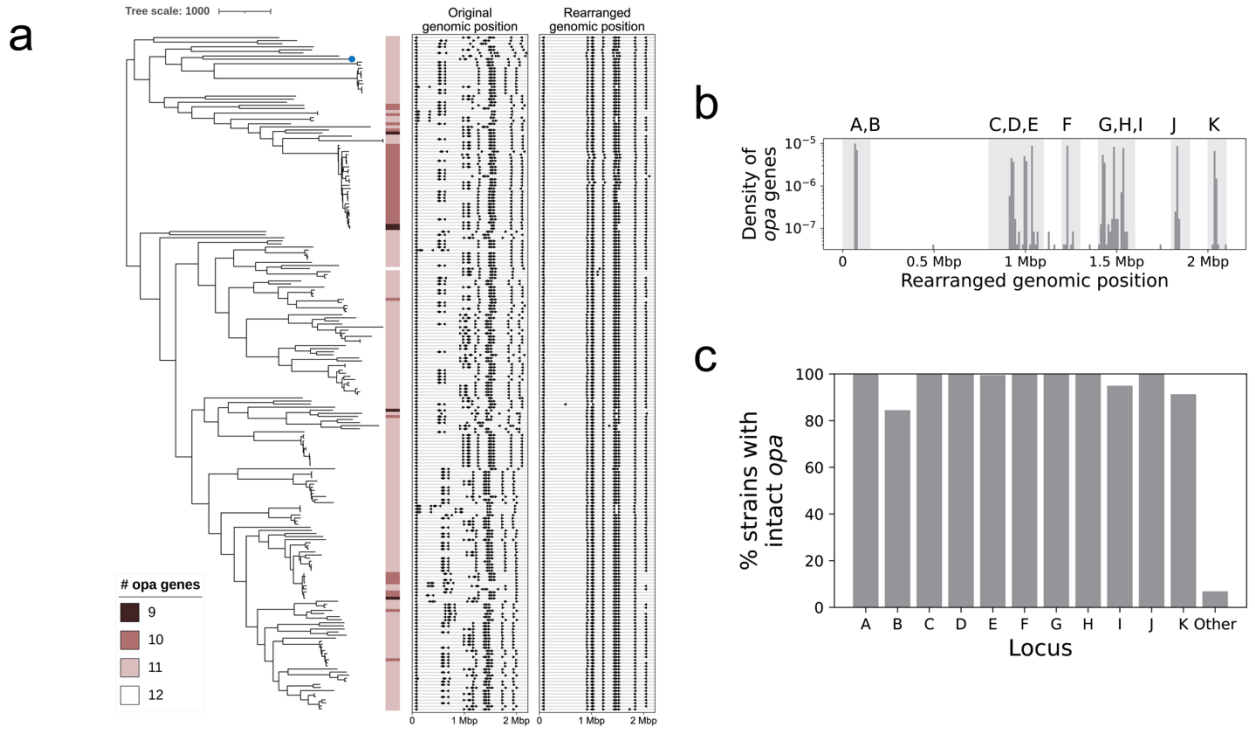

455

456

457 **Figure 2: Consistent local genomic positioning of *opa* reveals patterns of copy number**
458 **variation.** (a) Recombination-masked phylogeny of complete genomes annotated with the
459 number of intact *opa* genes (contain start codon, stop codon, and N-terminus) in each genome.
460 The genomic locations of the *opa* genes are shown in the middle panel and the rearranged
461 genomic locations of the *opa* genes are shown in the right panel. The reference genome
462 (FA1090) is shown with a blue dot on the phylogeny. The tree-scale indicates the number of
463 recombination-corrected SNPs. (b) The distribution of number of *opa* genes by rearranged
464 genomic position. The loci were named *opaA* to *opaK* based on the FA1090 genomic order. *opa*
465 genes that fell within the light-gray shaded background regions were assigned the
466 corresponding name(s). Where multiple *opa* genes occurred in proximity (for example, A and B;
467 C, D, and E; or G, H, and I), the *opa* genes within each genome were assigned in the order that
468 they appeared in the light-gray shaded region (i.e., the first *opa* gene is C, the second *opa* gene

469 is D, and the third *opa* gene is E). This was done to account for slight shifts in *opa* location
470 across genomes. (c) *opa* loci occupancy.
471
472 Diversity of *opa* alleles within genomes, across genomes, and compared with genome diversity
473
474 *opa* genes had almost as much within-isolate diversity as between-isolate diversity, as
475 measured by pairwise amino acid sequence identity (**Figure 3a**). The number of distinct *opa*
476 allele types per isolate, as defined by having less than 95% amino acid identity, ranged from 3
477 to 10, with a mean of 7 (**Figure 3c**). The Shannon diversity of *opa* types in each isolate ranged
478 from 1.03 to 2.27 with a mean of 1.84 (**Figure S 6**). There were more instances of similar *opa*
479 genes in the same isolate than in different isolates, and 96.8% (212/219) of isolates had at least
480 one pair of *opa* genes with more than 95% amino acid sequence identity (**Figure 3b**). One
481 isolate (NG250) had 7 *opa* genes with >95% amino acid sequence identity and three isolates
482 (CT213, TUM15748, and WHO_T_2024) each had 6 *opa* genes with >95% amino acid
483 sequence identity. Thirteen isolates had 4 pairs of *opa* genes with >95% amino acid sequence
484 identity (

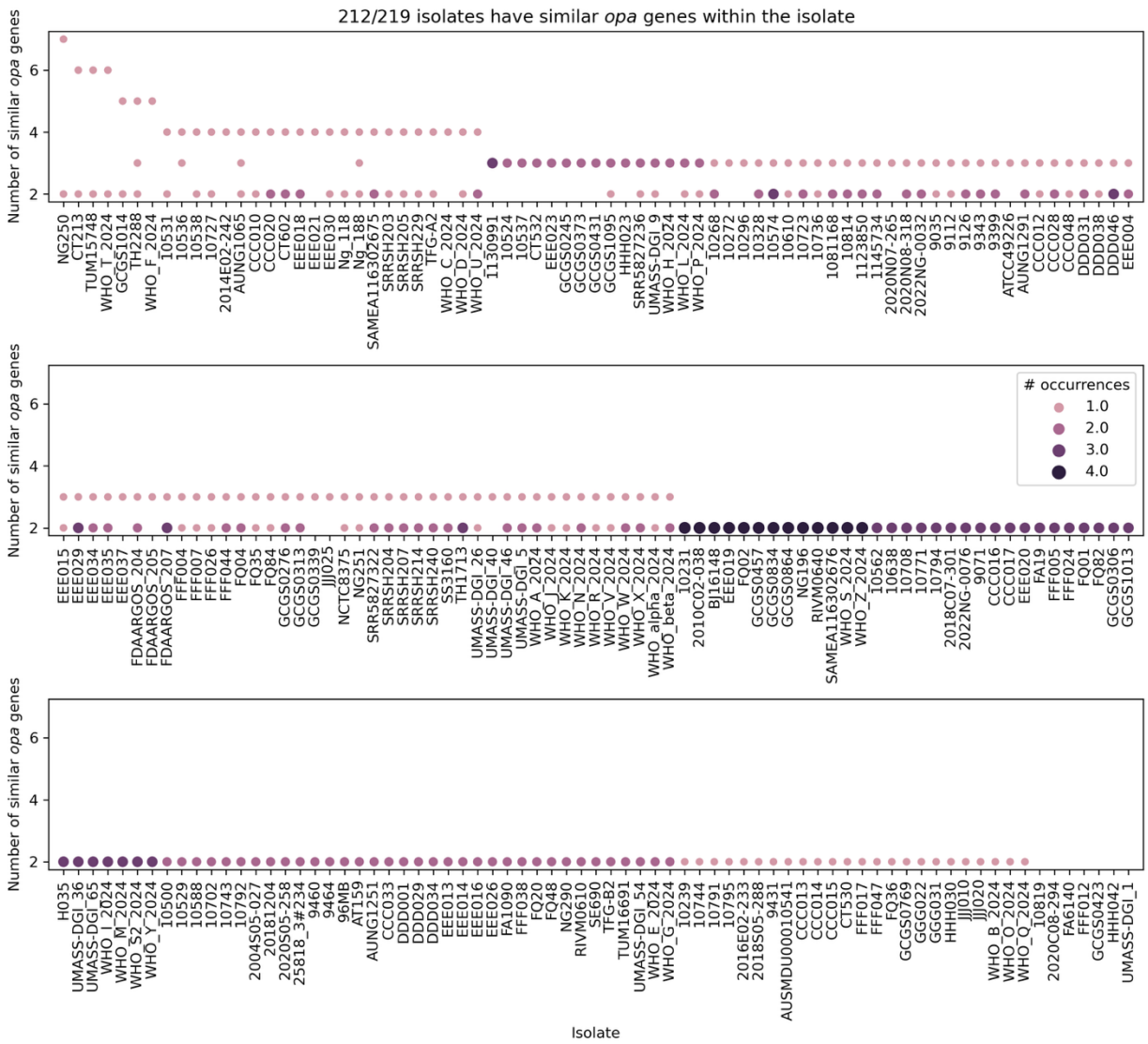

485

486 **Figure S 7**). *opa* sequence similarity correlated with genome similarity (Spearman correlation

487 coefficient 0.24, $p < 0.001$) (**Figure 3c**). In pairs of non-identical isolates, the number of sites in

488 the *opa* genes that differed was 13-3,294x higher (mean: 74x higher) than the number of whole

489 genome sites that differed, showing that *opa* genes are substantially more diverse than the rest

490 of the genome (**Figure 3d**).

491

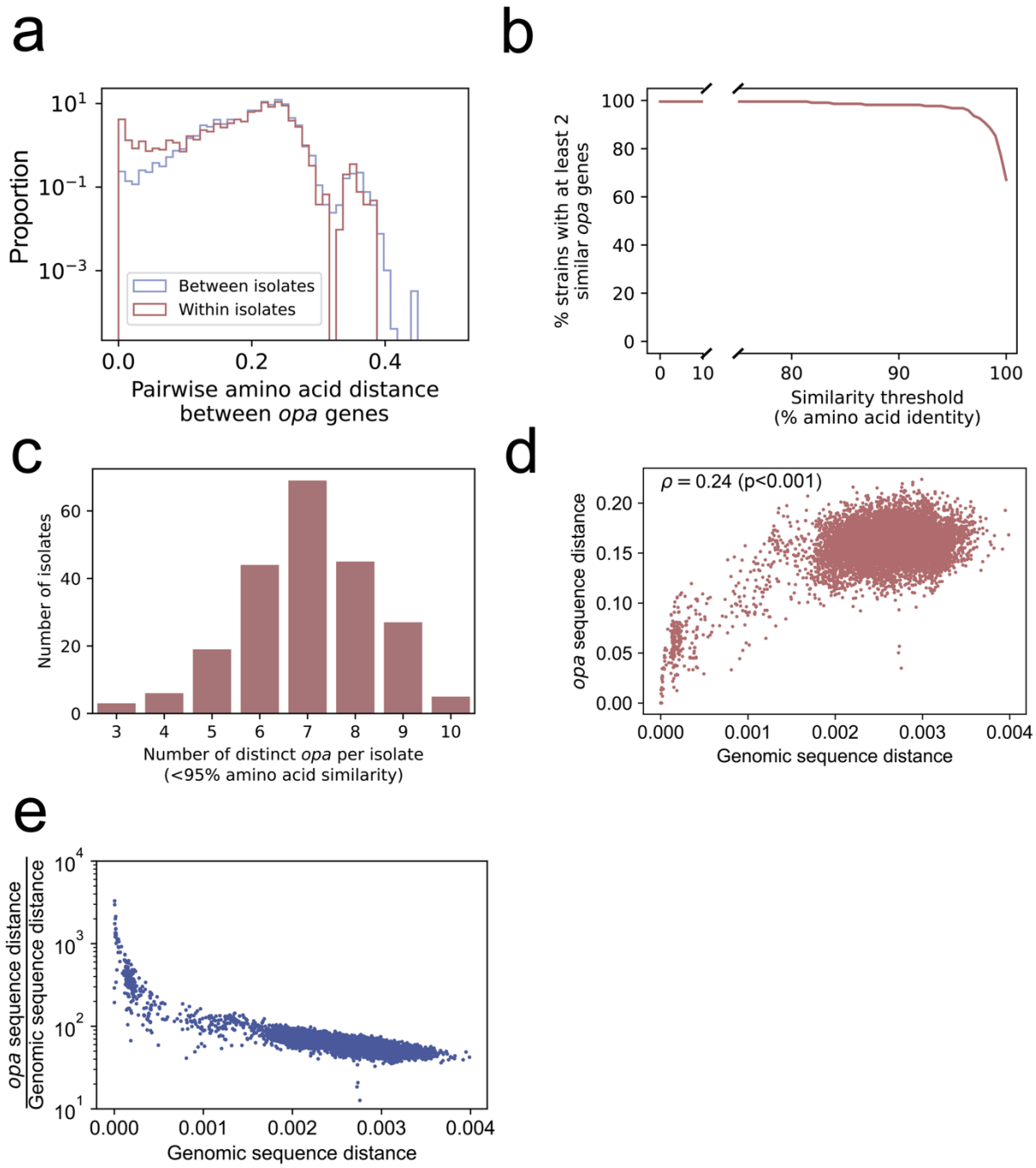

492

493

494 **Figure 3**: **Diversity of *opa* alleles within genomes, across genomes, and compared with**

495 **genome diversity.** (a) The distribution of the pairwise amino acid distance between *opa* genes

496 in the same isolate (red) and in different isolates (blue). The distribution of within-isolate *opa*

497 diversity was similar to the distribution of between-isolate *opa* diversity, except for the presence

498 of more near-identical *opa* genes in the same isolate. (b) The percentage of isolates with at
499 least 2 *opa* sequences above a given amino acid sequence identity. Nearly all (97.2%) isolates
500 have at least 2 *opa* sequences with >95% amino acid sequence identity. (c) The distribution of
501 the number of distinct *opa* allele types per isolate, defined as less than 95% amino acid
502 sequence identity. (d) Comparison of *opa* sequence distance and genomic sequence distance
503 in pairs of complete genomes with the same number of *opa* genes. Each point represents one
504 pair of complete genomes with the same number of *opa* genes. A distance of 0 indicates
505 identical, and a distance of 1 indicates every site is different. The Spearman correlation
506 coefficient and p-value are shown in the upper left. (e) The same data as in (d) but with the *opa*
507 sequence distance divided by the genomic sequence distance on the y axis.
508
509 <u>Fewer *opa* genes are in frame than expected by chance</u>
510
511 193/219 (88%) isolates had at least 1 *opa* gene in frame (**Figure 4**). The mean number of *opa*
512 genes in frame across all isolates was 1.7 and the maximum of *opa* genes in frame in any
513 isolate was 5. The mean number of in-frame *opa* genes per isolate was significantly lower
514 ($p<0.001$, Wilcoxon signed-rank test) than expected from a simple null model where each *opa*
515 has a 1/3 chance of being in frame (mean of 3.4 in-frame *opa* genes per isolate in null
516 distribution). *opa* genes that were more than 95% identical in amino acid sequence to at least
517 one other *opa* in the same isolate were 1.54 times less likely to be in frame than other *opa*
518 genes in the isolate ($p<10^{-4}$) (**Figure S 8**).
519

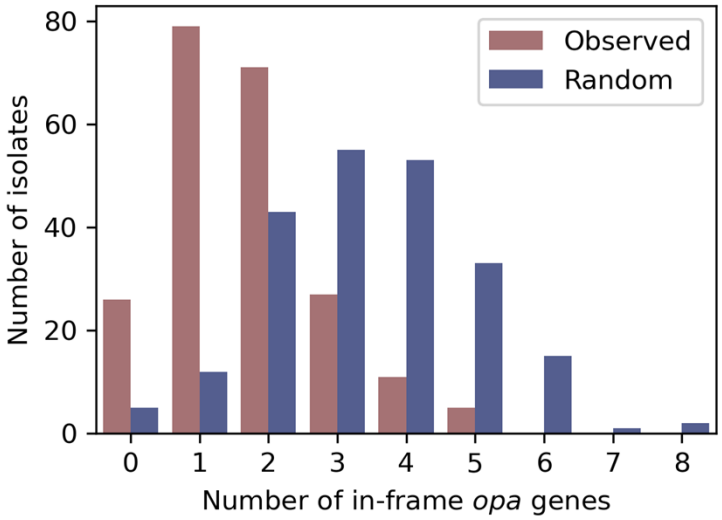

520

521 **Figure 4**: **Fewer *opa* genes are in frame than expected by chance.** The distribution of in-

522 frame *opa* genes per isolate.

523

524 *N. gonorrhoeae opa* are phylogenetically distinct from *Neisseria* species *opa*

525

526 As *N. gonorrhoeae* can gain new genetic diversity through interspecies mosaicism [56,57], we

527 evaluated the possible contribution of other *Neisseria* to *N. gonorrhoeae opa* diversity (**Figure S**

528 **9**). Our approach to searching for the *opa* genes in *Neisseria* species using conserved

529 sequences identified the same number of intact *opa* genes as BLAST, and BLAST identified

530 one additional truncated *opa* gene. Most *N. meningitidis* isolates had 4 full length *opa* (115/136

531 isolates), and more rarely 3 full length *opa* (19/136 isolates) or 5 full length *opa* (2/136 isolates).

532 *N. flavescens* and *N. lactamica* isolates had 2 full length *opa* (1 isolate of *N. flavescens* and 4

533 isolates of *N. lactamica*), and *N. polysaccharea* had 1 full length *opa* (1 isolate) (**Figure 5a**).

534 Multiple *Neisseria* species had partial *opa* genes that contained the C-terminal region of the *opa*

535 gene only: *N. animalis* (2 isolates with 2 partial *opa* each), *N. arctica* (1 isolate with 2 partial

536 *opa*), *N. brasiliensis* (1 isolate with 1 partial *opa*), *N. sicca* (1 isolate with 1 partial *opa*, 2 isolates

537 with no *opa*), *and N. zalophi* (1 isolate with 1 partial *opa*). Additionally, 11/136 *N. meningitidis*

538 isolates had a partial *opa* which all have the same sequence (including the upstream region). *N.*
539 *gonorrhoeae opa* were phylogenetically distinct from *opa* from other *Neisseria* species, except
540 for one allele, which was found in 8 *N. gonorrhoeae* isolates. This allele clustered with, and its
541 sequence was similar to, commensal *Neisseria opa* (**Figure 5b**).
542
543

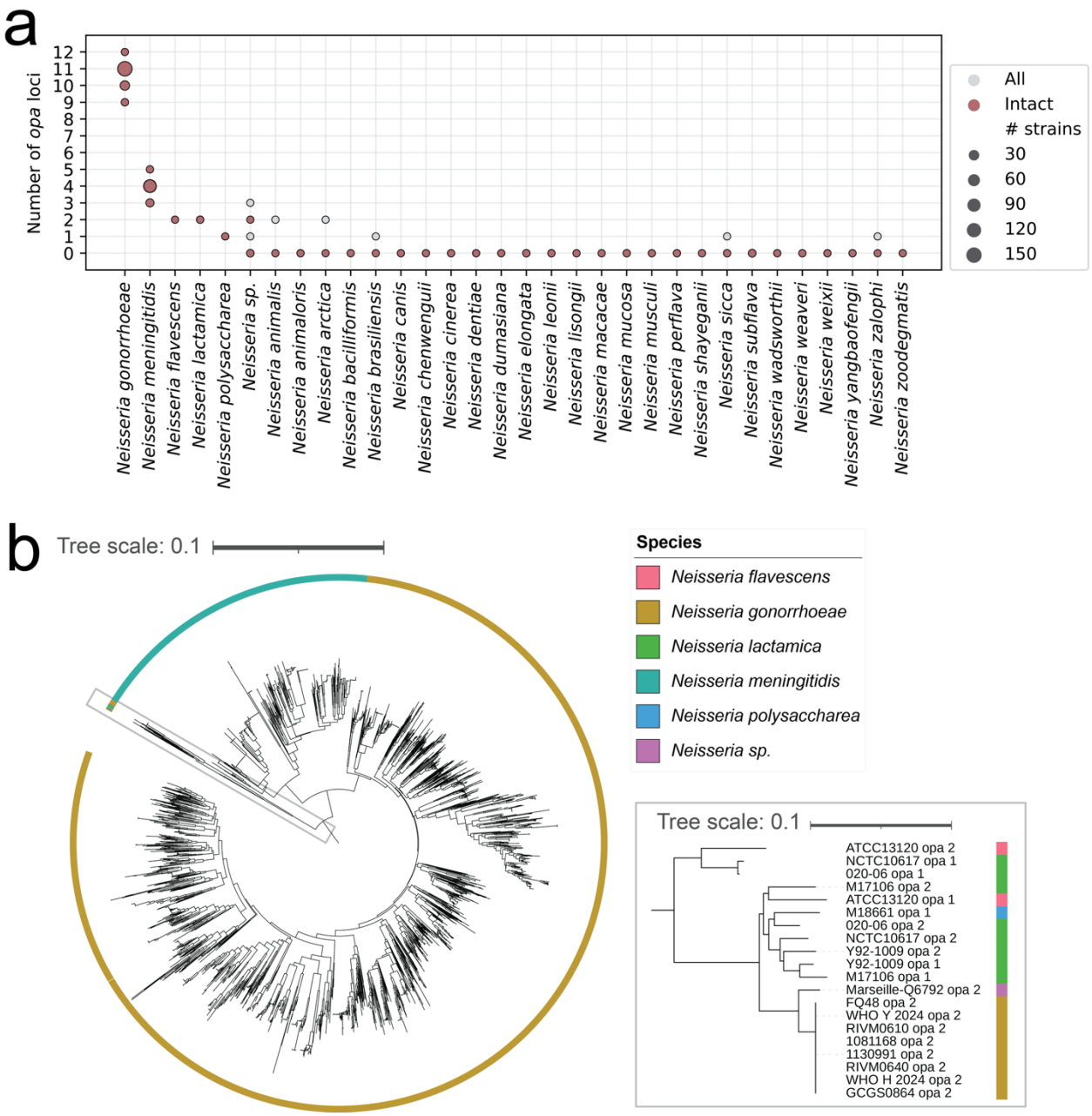

544

545

546 **Figure 5**: ***N. gonorrhoeae opa* are phylogenetically distinct from other *Neisseria* species**
547 ***opa*.** (a) The distribution of the total (partial and intact) and intact number of *opa* loci by species.
548 (b) k-mer distance-based neighbor-joining phylogeny of the *opa* sequences in all *Neisseria*
549 species. *N. gonorrhoeae opa* are phylogenetically distinct from *opa* sequences from other
550 *Neisseria* species, with the exception of one allele that clustered with other *Neisseria* species
551 *opa* (inset, which shows zoom of the boxed section of the phylogeny). The tree scales indicate
552 the k-mer distance.

553

554 <u>The rate of *opa* evolution is dependent on the genetic locus</u>

555

556 To estimate the rate of evolution, we first clustered *opa* by sequence similarity (**Figure S 10**).
557 Because of known recombination-mediated shuffling [10,11] of the semivariable, hypervariable
558 1, and hypervariable 2 sequences (**Figure S 10a**), we clustered each of these regions
559 separately using k-mer distances and a network clustering approach (**Figure S 10b**). The
560 clustering resulted in 6 semivariable region clusters, 21 hypervariable 1 region clusters, and 9
561 hypervariable 2 region clusters (**Figure S 10c**). The nucleotide k-mer distances for sequences
562 in the same cluster are lower than the distances for sequences in different clusters (**Figure S**
563 **11**), and examination of the sequences shows that each cluster has a distinct motif (**Figure S**
564 **12-14**).

565

566 We reconstructed the ancestral states of the *opa* cluster types on a dated phylogeny to estimate
567 the rate of *opa* evolution. We focused on the only clade in the phylogeny of complete genomes
568 that had densely sampled isolates (branch length less than 200 recombination-corrected
569 mutations and more than 20 samples) (**Figure 6a**). The inferred substitution rate, 3.1×10^{-6}

570 [1.7×10^{-6}, 4.4×10^{-6}] substitutions per chromosome per year, fell within the rate expected for *N.*

571 *gonorrhoeae* [58]. The rate of cluster type changes was substantially higher for *opaK* compared

572 to the other *opa* loci (**Figure 6b**). The cluster types that appeared in *opaA* and *opaK* were

573 similar, showing that the difference in the rates of cluster type changes between the two loci

574 was due to different rates of shuffling between the same cluster types (**Figure S 15**). *opaK* was

575 not significantly more in frame than the other *opa* loci (**Figure S 16**).

576

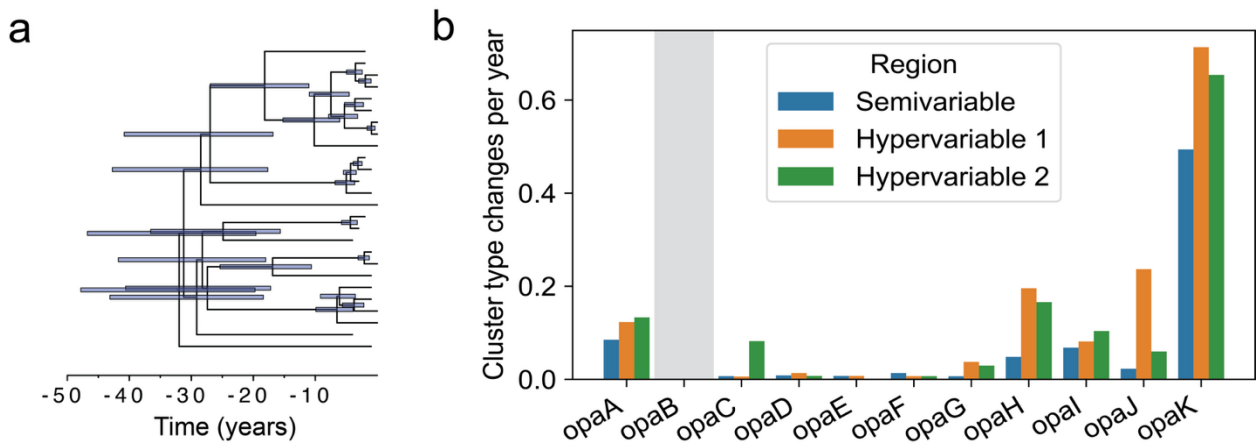

577

578

579 **Figure 6**: **The rate of *opa* evolution is dependent on the genetic locus**. (a) Dated phylogeny

580 of the clade in **Figure 2a** with densely sampled isolates (branch length less than 200

581 recombination-corrected mutations and more than 20 samples). Error bars represent the 95%

582 highest posterior density of the node heights. (b) Rate of semivariable, hypervariable 1, and

583 hypervariable 2 cluster type changes by *opa* locus for subtree depicted in (a). The gray shaded

584 region denotes that *opaB* was missing from all isolates in this subtree. In other loci, there were

585 no more than 2 isolates missing each *opa*.

586

587 <u>Correlation of hypervariable 1 and hypervariable 2 region alleles</u>

588

589 Using the cluster typing, we were also able to assess whether certain hypervariable 1 and
590 hypervariable 2 alleles appeared together more often than expected by chance (**Figure S 17**).
591 We accounted for isolate sampling and population structure by randomly sampling 1 isolate per
592 whole genome cluster 100 times. For each subset of representative isolates, out of 100
593 randomizations of the data, the actual data always showed higher levels of association between
594 hypervariable types than the randomized data.
595
596 **Discussion**
597
598 Quantitative assessment of *opa* diversity, expression, and evolution
599
600 Prior to this study, there were several open questions about *opa* genes in *N. gonorrhoeae*: how
601 are *opa* genes organized in the genome? Are there patterns in their diversity and expression?
602 How much *opa* diversity is there in the population? How do *opa* evolve? Here, we have
603 advanced our understanding for each of these questions using a new diverse dataset of
604 complete *N. gonorrhoeae* genomes.
605
606 *Genomic rearrangements shuffle* opa *position*
607
608 Genomic rearrangements shuffle *opa* position in the genome, but by accounting for them, we
609 were able to assign consistent *opa* loci. Genomic rearrangements in closely related isolates
610 happened very rarely, but there is space for the locus assignment approach to be updated if we
611 see more examples of genomic rearrangements in closely related isolates.
612
613 *Gain and loss of* opa *occurred repeatedly*
614

While most isolates had 11 *opa* genes, we found a handful of instances of *opa* loss and gain. The loss events occurred across the phylogeny. In some instances, we saw examples of the gene loss events passed on to progeny. More than 50% of these loss events were explained by truncated *opa* genes. We were unable to identify the mechanism for the other loss events. Furthermore, in intact *opa* sequences, we observed frameshift mutations occurring downstream of the coding repeat sequence leading to a premature stop codon, but we were unable to determine how many of these frameshift mutations were due to sequencing error. In one isolate, we identified 12 *opa* genes, which seemed to be due to a recent genomic duplication event that exactly duplicated another *opa* gene in the genome. The fact that we only observed one isolate with 12 *opa* suggests that the expansion of *opa* number is rare.

Within-isolate opa *diversity is generally high, with some exceptions*

The diversity of *opa* alleles within isolates was generally high, with the average isolate having 7 distinct *opa* alleles, but there were some isolates with as few as 3 distinct *opa* alleles. This suggests that there is some pressure to have diverse *opa* alleles within an isolate. At the same time, almost all isolates had at least two near-identical *opa* alleles, possibly as a result of gene conversion, suggesting there may be a balance between maintaining diversity and maintaining function while diversifying.

Fewer opa *expressed than expected by chance*

Across the population, fewer *opa* appeared to be expressed based on the sequence than expected by chance. Furthermore, near-identical *opa* genes in the same isolate tended to be out of frame more often than unique *opa* genes. Our results suggest mechanisms other than chance alone in guiding the patterns of phase variation, for example, regulation of changes in

641 repeat number or selection against isolates with many *opa* alleles being expressed. While these
642 mechanisms are yet unknown, previous work suggested that promoter strength may play a role
643 in regulating *opa* phase [59] and there may be selection against *opa* expression in certain
644 environments, for example the presence of progesterone [60–62].
645
646 opa *diversity is correlated with and higher than genome diversity*
647
648 *opa* genes are on average 74 times more diverse than the rest of the genome. More closely-
649 related isolates have more similar *opa* sequence repertoires. In the context of reinfections, our
650 results suggest that when reinfections occur with the same or a closely related isolate, there will
651 be a similar *opa* repertoire. We speculate that if there is immunological memory to the *opa* that
652 are expressed, then different *opa* are turned on in subsequent reinfections, an idea that is also
653 supported by evidence of variation in *opa* expression over the course of single infections in
654 human challenge studies [63,64]. When reinfections occur with different isolates, there will likely
655 be different *opa* alleles expressed.
656
657 *Interspecies recombination does not appear to play a large role in generation of* opa *diversity*
658
659 *N. gonorrhoeae opa* allelic diversity did not overlap with *opa* from other *Neisseria* species. While
660 sequencing more complete genomes may lead to more observations of interspecies mosaicism,
661 the separate clustering of *N. gonorrhoeae* and *N. meningitidis opa* in our dataset and in Malorny
662 et al. [9] suggests phylogenetic separation of *opa* sequences between species. The separate
663 clustering of *Neisseria* species *opa* may be due to the different functional constraints of host
664 receptor binding or differences in flanking regions of *opa* genes from different species that
665 prevent homologous recombination from occurring between species.
666

667 *Variation in rate of* opa *variation across loci*

668

669 *opaK* varies more rapidly than other loci, but it is not significantly more in frame in our dataset.
670 The differences in rates of evolution by *opa* locus may be due to variability in the accessibility of
671 each locus for recombination or other diversity generating processes (i.e., structural
672 accessibility). The changes in *opaK* tend to reflect recombination among existing *opa* types,
673 suggesting that diversity is mostly generated through shuffling of existing sequences. Bilek et al.
674 [21] suggested a possible connection between *opa11* (*opaK* in this study) variation and the
675 neighboring *pilE* Pilin expression gene variation, but noted this may not be causal.

676

677 *Hypervariable region 1 and 2 alleles are more correlated than expected by chance*

678

679 Hypervariable region 1 and 2 alleles in *N. meningitidis* are more correlated than expected due to
680 chance [65]. We showed that this phenomenon also occurs in *N. gonorrhoeae*. The non-random
681 association of hypervariable alleles is consistent with predictions of a mathematical model of
682 strong immune selection [66], physical linkage on the chromosome, and selection for particular
683 combinations of hypervariable alleles for functional reasons (i.e., to bind to specific host
684 receptors)[67].

685

686 <u>Limitations of our study</u>

687

688 There are several limitations to our study. First, the number of complete genomes sequenced
689 was limited, possibly missing some *opa* diversity. Second, gonococcal passaging during
690 culturing may have changed the phase of *opa* genes. Culture-independent sequencing that
691 resolves *opa* phase *in vivo* will add to our understanding of patterns of *opa* expression. Third,
692 there is limited data on *opa* function, with only a few *opa* sequences characterized for their

693 binding to host receptors and antibody recognition [15]. While the clustering nomenclature for
694 *opa* that we developed is entirely sequence based, we expect closely related sequences to
695 have more closely related functions on average. In the future, functional data can be
696 incorporated to refine the *opa* clustering definitions. Fourth, we were limited in the estimation of
697 the rate of evolution to only a single densely sampled subtree. There may be differences in the
698 rate of *opa* evolution across genomic backgrounds.
699
700 Model
701
702 Taken together, our results support a model of *opa* variation where on short timescales phase
703 variation modulates the translation of highly diverse *opa* alleles, typically with very few *opa*
704 being expressed at one time. On long timescales, recombination, gene conversion, mutation,
705 and gene gain and loss lead to changes in the *opa* repertoire, with the rate of these processes
706 dependent on the genetic locus (**Figure 7**). The rapid rate of phase variation and diversification
707 will likely lead hosts to be exposed to different Opa types upon reinfection and may allow
708 antigenic escape in vivo in chronic or undiagnosed infections.
709
710

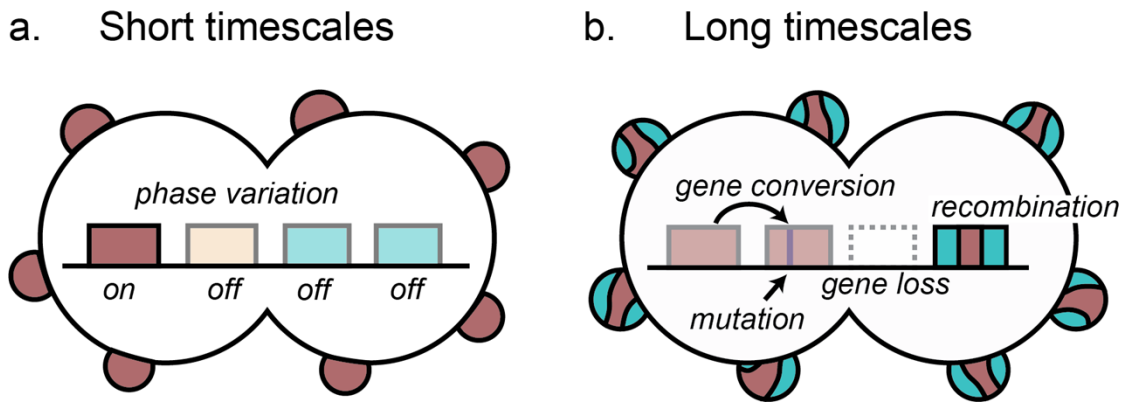

711
712

713 **Figure 7**: **Model of *opa* variation and evolution supported by our results.** (a) On short
714 timescales, phase variation modulates the expression of highly diverse *opa* alleles within
715 isolates, typically with very few *opa* being expressed at one time. (b) On long timescales,
716 recombination, gene conversion, mutation, and gene gain and loss within species in a locus-
717 dependent manner lead to changes in the *opa* repertoire.
718

719 **Acknowledgements**

720 We are grateful to Eric Neubauer Vickers for helpful discussions and comments on the
721 manuscript. We are grateful to the Grad lab and the Center for Communicable Disease
722 Dynamics for helpful discussions. This project received support from the American Sexually
723 Transmitted Diseases Association (to YHG and QY), NIH R21 AI172369 (to YHG), and NIH T32
724 AI007535 (to QY). The computations in this paper were run on the FASRC Cannon cluster
725 supported by the FAS Division of Science Research Computing Group at Harvard University.
726

727 **References**

728

729 1. WHO bacterial priority pathogens list, 2024: Bacterial pathogens of public health
730 importance to guide research, development and strategies to prevent and control
731 antimicrobial resistance. World Health Organization; 17 May 2024 [cited 12 Aug 2025].
732 Available: https://www.who.int/publications/i/item/9789240093461

733 2. Unemo M, Seifert HS, Hook EW 3rd, Hawkes S, Ndowa F, Dillon J-AR. Gonorrhoea. Nat
734 Rev Dis Primers. 2019;5: 79.

735 3. Schmidt KA, Schneider H, Lindstrom JA, Boslego JW, Warren RA, Van de Verg L, et al.
736 Experimental gonococcal urethritis and reinfection with homologous gonococci in male
737 volunteers. Sex Transm Dis. 2001;28: 555–564.

738 4. Belcher T, Rollier CS, Dold C, Ross JDC, MacLennan CA. Immune responses to Neisseria
739 gonorrhoeae and implications for vaccine development. Front Immunol. 2023;14: 1248613.

740 5. Fox KK, Thomas JC, Weiner DH, Davis RH, Sparling PF, Cohen MS. Longitudinal
741 evaluation of serovar-specific immunity to Neisseria gonorrhoeae. Am J Epidemiol.
742 1999;149: 353–358.

743 6. de Korne-Elenbaas J, Bruisten SM, de Vries HJC, van Dam AP. Within-Host Genetic
744 Variation in Neisseria gonorrhoeae over the Course of Infection. Microbiol Spectr. 2022;10:
745 e0031322.

746 7. Quillin SJ, Seifert HS. Neisseria gonorrhoeae host adaptation and pathogenesis. Nat Rev
747 Microbiol. 2018;16: 226–240.

748 8. Black WJ, Schwalbe RS, Nachamkin I, Cannon JG. Characterization of Neisseria
749 gonorrhoeae protein II phase variation by use of monoclonal antibodies. Infect Immun.
750 1984;45: 453–457.

751 9. Malorny B, Morelli G, Kusecek B, Kolberg J, Achtman M. Sequence diversity, predicted
752 two-dimensional protein structure, and epitope mapping of neisserial Opa proteins. J
753 Bacteriol. 1998;180: 1323–1330.

754 10. Dempsey JA, Litaker W, Madhure A, Snodgrass TL, Cannon JG. Physical map of the
755 chromosome of Neisseria gonorrhoeae FA1090 with locations of genetic markers, including
756 opa and pil genes. J Bacteriol. 1991;173: 5476–5486.

757 11. Connell TD, Black WJ, Kawula TH, Barritt DS, Dempsey JA, Kverneland K Jr, et al.
758 Recombination among protein II genes of Neisseria gonorrhoeae generates new coding
759 sequences and increases structural variability in the protein II family. Mol Microbiol. 1988;2:
760 227–236.

761 12. Chen T, Belland RJ, Wilson J, Swanson J. Adherence of pilus- Opa+ gonococci to epithelial
762 cells in vitro involves heparan sulfate. J Exp Med. 1995;182: 511–517.

763 13. van Putten JP, Paul SM. Binding of syndecan-like cell surface proteoglycan receptors is
764 required for Neisseria gonorrhoeae entry into human mucosal cells. EMBO J. 1995;14:
765 2144–2154.

766 14. Virji M, Evans D, Hadfield A, Grunert F, Teixeira AM, Watt SM. Critical determinants of host
767 receptor targeting by Neisseria meningitidis and Neisseria gonorrhoeae: identification of
768 Opa adhesiotopes on the N-domain of CD66 molecules. Mol Microbiol. 1999;34: 538–551.

769 15. Sadarangani M, Pollard AJ, Gray-Owen SD. Opa proteins and CEACAMs: pathways of
770 immune engagement for pathogenic Neisseria. FEMS Microbiol Rev. 2011;35: 498–514.

771 16. Gómez-Duarte OG, Dehio M, Guzmán CA, Chhatwal GS, Dehio C, Meyer TF. Binding of
772 vitronectin to opa-expressing Neisseria gonorrhoeae mediates invasion of HeLa cells. Infect
773 Immun. 1997;65: 3857–3866.

774 17. Duensing TD, van Putten JP. Vitronectin mediates internalization of Neisseria gonorrhoeae
775 by Chinese hamster ovary cells. Infect Immun. 1997;65: 964–970.

776 18. Pantelic M, Kim Y-J, Bolland S, Chen I, Shively J, Chen T. Neisseria gonorrhoeae kills
777 carcinoembryonic antigen-related cellular adhesion molecule 1 (CD66a)-expressing human
778 B cells and inhibits antibody production. Infect Immun. 2005;73: 4171–4179.

779 19. Bhat KS, Gibbs CP, Barrera O, Morrison SG, Jähnig F, Stern A, et al. The opacity proteins
780 of Neisseria gonorrhoeae strain MS11 are encoded by a family of 11 complete genes. Mol
781 Microbiol. 1991;5: 1889–1901.

782 20. Stern A, Brown M, Nickel P, Meyer TF. Opacity genes in Neisseria gonorrhoeae: control of
783 phase and antigenic variation. Cell. 1986;47: 61–71.

784 21. Bilek N, Ison CA, Spratt BG. Relative contributions of recombination and mutation to the
785 diversification of the opa gene repertoire of Neisseria gonorrhoeae. J Bacteriol. 2009;191:
786 1878–1890.

787 22. van der Ley P. Three copies of a single protein II-encoding sequence in the genome of
788 Neisseria gonorrhoeae JS3: evidence for gene conversion and gene duplication. Mol
789 Microbiol. 1988;2: 797–806.

790 23. Kellogg DS Jr, Peacock WL Jr, Deacon WE, Brown L, Pirkle CI. Neisseria gonorrhoeae i. J
791 Bacteriol. 1963;85: 1274–1279.

792 24. Oxford Nanopore Technologies. Dorado. 2024. Available:
793 https://github.com/nanoporetech/dorado

794 25. Wick RR, Howden BP, Stinear TP. Autocycler: long-read consensus assembly for bacterial
795 genomes. bioRxiv. 2025. p. 2025.05.12.653612. doi:10.1101/2025.05.12.653612

796 26. Koren S, Walenz BP, Berlin K, Miller JR, Bergman NH, Phillippy AM. Canu: scalable and
797 accurate long-read assembly via adaptive k-mer weighting and repeat separation. Genome
798 Res. 2017;27: 722–736.

799 27. Kolmogorov M, Yuan J, Lin Y, Pevzner PA. Assembly of long, error-prone reads using
800 repeat graphs. Nat Biotechnol. 2019;37: 540–546.

801 28. Li H. Minimap and miniasm: fast mapping and de novo assembly for noisy long sequences.
802 Bioinformatics. 2016;32: 2103–2110.

803 29. Chen Y, Nie F, Xie S-Q, Zheng Y-F, Dai Q, Bray T, et al. Efficient assembly of nanopore
804 reads via highly accurate and intact error correction. Nat Commun. 2021;12: 60.

805 30. Hu J, Wang Z, Sun Z, Hu B, Ayoola AO, Liang F, et al. NextDenovo: an efficient error
806 correction and accurate assembly tool for noisy long reads. Genome Biol. 2024;25: 107.

807 31. Vaser R, Šikić M. Time- and memory-efficient genome assembly with Raven. Nat Comput
808 Sci. 2021;1: 332–336.

809 32. Durbin R, De Sanctis B, Blumer M. Rotate: A command-line program to rotate circular DNA
810 sequences to start at a given position or string. Wellcome Open Res. 2023;8: 401.

811 33. Seemann T. Prokka: rapid prokaryotic genome annotation. Bioinformatics. 2014;30: 2068–
812 2069.

813 34. Page AJ, Cummins CA, Hunt M, Wong VK, Reuter S, Holden MTG, et al. Roary: rapid
814 large-scale prokaryote pan genome analysis. Bioinformatics. 2015;31: 3691–3693.

815 35. Katoh K, Standley DM. MAFFT multiple sequence alignment software version 7:
816 improvements in performance and usability. Mol Biol Evol. 2013;30: 772–780.

817 36. Waterhouse AM, Procter JB, Martin DMA, Clamp M, Barton GJ. Jalview Version 2--a
818 multiple sequence alignment editor and analysis workbench. Bioinformatics. 2009;25:
819 1189–1191.

820 37. Darling AE, Mau B, Perna NT. progressiveMauve: multiple genome alignment with gene
821 gain, loss and rearrangement. PLoS One. 2010;5: e11147.

822 38. Huang W, Li L, Myers JR, Marth GT. ART: a next-generation sequencing read simulator.
823 Bioinformatics. 2012;28: 593–594.

824 39. Li H. Aligning sequence reads, clone sequences and assembly contigs with BWA-MEM.
825 arXiv [q-bio.GN]. 2013. Available: http://arxiv.org/abs/1303.3997

826 40. Danecek P, Bonfield JK, Liddle J, Marshall J, Ohan V, Pollard MO, et al. Twelve years of
827 SAMtools and BCFtools. Gigascience. 2021;10. doi:10.1093/gigascience/giab008

828 41. Okonechnikov K, Conesa A, García-Alcalde F. Qualimap 2: advanced multi-sample quality
829 control for high-throughput sequencing data. Bioinformatics. 2016;32: 292–294.

830 42. Walker BJ, Abeel T, Shea T, Priest M, Abouelliel A, Sakthikumar S, et al. Pilon: an
831 integrated tool for comprehensive microbial variant detection and genome assembly
832 improvement. PLoS One. 2014;9: e112963.

833 43. Lees JA, Harris SR, Tonkin-Hill G, Gladstone RA, Lo SW, Weiser JN, et al. Fast and
834 flexible bacterial genomic epidemiology with PopPUNK. Genome Res. 2019;29: 304–316.

835 44. Croucher NJ, Page AJ, Connor TR, Delaney AJ, Keane JA, Bentley SD, et al. Rapid
836 phylogenetic analysis of large samples of recombinant bacterial whole genome sequences
837 using Gubbins. Nucleic Acids Res. 2015;43: e15.

838 45. Kozlov AM, Darriba D, Flouri T, Morel B, Stamatakis A. RAxML-NG: a fast, scalable and
839 user-friendly tool for maximum likelihood phylogenetic inference. Bioinformatics. 2019;35:
840 4453–4455.

841 46. Ondov BD, Treangen TJ, Melsted P, Mallonee AB, Bergman NH, Koren S, et al. Mash: fast
842 genome and metagenome distance estimation using MinHash. Genome Biol. 2016;17: 132.

843 47. Simonsen M, Mailund T, Pedersen CNS. Rapid neighbour-joining. Lecture Notes in
844 Computer Science. Berlin, Heidelberg: Springer Berlin Heidelberg; 2008. pp. 113–122.

845 48. Van Dongen S. Graph clustering via a discrete uncoupling process. SIAM J Matrix Anal
846 Appl. 2008;30: 121–141.

847 49. Enright AJ, Van Dongen S, Ouzounis CA. An efficient algorithm for large-scale detection of
848 protein families. Nucleic Acids Res. 2002;30: 1575–1584.

849 50. Tareen A, Kinney JB. Logomaker: beautiful sequence logos in Python. Bioinformatics.
850 2020;36: 2272–2274.

851 51. Bouckaert R, Vaughan TG, Barido-Sottani J, Duchêne S, Fourment M, Gavryushkina A, et
852 al. BEAST 2.5: An advanced software platform for Bayesian evolutionary analysis. PLoS
853 Comput Biol. 2019;15: e1006650.

854 52. Ishikawa SA, Zhukova A, Iwasaki W, Gascuel O. A fast likelihood method to reconstruct
855 and visualize ancestral scenarios. Mol Biol Evol. 2019;36: 2069–2085.

856 53. Letunic I, Bork P. Interactive Tree of Life (iTOL) v6: recent updates to the phylogenetic tree
857 display and annotation tool. Nucleic Acids Res. 2024;52: W78–W82.

858 54. Köster J, Rahmann S. Snakemake--a scalable bioinformatics workflow engine.
859 Bioinformatics. 2012;28: 2520–2522.

860 55. Unemo M, Sánchez-Busó L, Golparian D, Jacobsson S, Shimuta K, Lan PT, et al. The
861 novel 2024 WHO Neisseria gonorrhoeae reference strains for global quality assurance of
862 laboratory investigations and superseded WHO N. gonorrhoeae reference strains-
863 phenotypic, genetic and reference genome characterization. J Antimicrob Chemother.
864 2024. doi:10.1093/jac/dkae176

865 56. Wadsworth CB, Arnold BJ, Sater MRA, Grad YH. Azithromycin Resistance through
866 Interspecific Acquisition of an Epistasis-Dependent Efflux Pump Component and

867 Transcriptional Regulator in Neisseria gonorrhoeae. MBio. 2018;9.
868 doi:10.1128/mBio.01419-18

869 57. Unitt A, Maiden M, Harrison O. Characterizing the diversity and commensal origins of penA
870 mosaicism in the genus Neisseria. Microb Genom. 2024;10. doi:10.1099/mgen.0.001209

871 58. Grad YH, Kirkcaldy RD, Trees D, Dordel J, Harris SR, Goldstein E, et al. Genomic
872 epidemiology of Neisseria gonorrhoeae with reduced susceptibility to cefixime in the USA: a
873 retrospective observational study. Lancet Infect Dis. 2014;14: 220–226.

874 59. Belland RJ, Morrison SG, Carlson JH, Hogan DM. Promoter strength influences phase
875 variation of neisserial opa genes. Mol Microbiol. 1997;23: 123–135.

876 60. James JF, Swanson J. Studies on gonococcus infection. XIII. Occurrence of color/opacity
877 colonial variants in clinical cultures. Infect Immun. 1978;19: 332–340.

878 61. James JF, Swanson J. Color/opacity colonial variants of Neisseria gonorrhoeae and their
879 relationship to the menstrual cycle. In: G. F. Brooks, E. C. Gotschlich, K. K. Holmes, W. D.
880 Sawyer, and F. E. Young, editor. Immunobiology of Neisseria gonorrhoeae. Annals of
881 Internal Medicine; 1978. pp. 338–343.

882 62. Salit IE. The differential susceptibility of gonococcal opacity variants to sex hormones. Can
883 J Microbiol. 1982;28: 301–306.

884 63. Jerse AE, Cohen MS, Drown PM, Whicker LG, Isbey SF, Seifert HS, et al. Multiple
885 gonococcal opacity proteins are expressed during experimental urethral infection in the
886 male. J Exp Med. 1994;179: 911–920.

887 64. Swanson J, Barrera O, Sola J, Boslego J. Expression of outer membrane protein II by
888 gonococci in experimental gonorrhea. J Exp Med. 1988;168: 2121–2129.

889 65. Callaghan MJ, Jolley KA, Maiden MCJ. Opacity-associated adhesin repertoire in
890 hyperinvasive Neisseria meningitidis. Infect Immun. 2006;74: 5085–5094.

891 66. Callaghan MJ, Buckee CO, Jolley KA, Kriz P, Maiden MCJ, Gupta S. The effect of immune
892 selection on the structure of the meningococcal opa protein repertoire. PLoS Pathog.
893 2008;4: e1000020.

894 67. Bos MP, Kao D, Hogan DM, Grant CCR, Belland RJ. Carcinoembryonic antigen family
895 receptor recognition by gonococcal Opa proteins requires distinct combinations of
896 hypervariable Opa protein domains. Infect Immun. 2002;70: 1715–1723.

897 68. Bristow CC, Mortimer TD, Morris S, Grad YH, Soge OO, Wakatake E, et al. Whole-genome
898 sequencing to predict antimicrobial susceptibility profiles in Neisseria gonorrhoeae. J Infect
899 Dis. 2023;227: 917–925.

900 69. Bouras G, Judd LM, Edwards RA, Vreugde S, Stinear TP, Wick RR. How low can you go?
901 Short-read polishing of Oxford Nanopore bacterial genome assemblies. bioRxiv. 2024. p.
902 2024.03.07.584013. doi:10.1101/2024.03.07.584013

903 70. Menardo F, Loiseau C, Brites D, Coscolla M, Gygli SM, Rutaihwa LK, et al. Treemmer: a
904 tool to reduce large phylogenetic datasets with minimal loss of diversity. BMC
905 Bioinformatics. 2018;19: 164.

906 71. Tonkin-Hill G, Lees JA, Bentley SD, Frost SDW, Corander J. Fast hierarchical Bayesian
907 analysis of population structure. Nucleic Acids Res. 2019;47: 5539–5549.

908

909 **Supplementary figures**

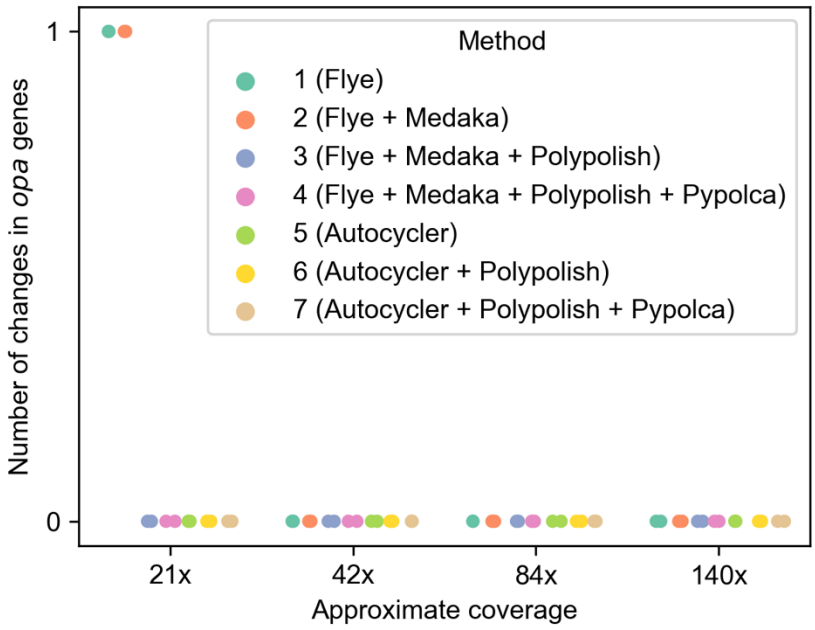

910

911 **Figure S 1: Comparison of *opa* sequences across long-read assembly and polishing**

912 **methods**. The number of changes in *opa* genes at 4 read coverage levels using 7 different

913 assembly and polishing procedures. There are two points of the same color in each coverage

914 level, indicating two different isolates. The changes at 21x for methods 1 and 2 include one SNP

915 in one isolate's genome and one single base insertion in the other isolate's genome.

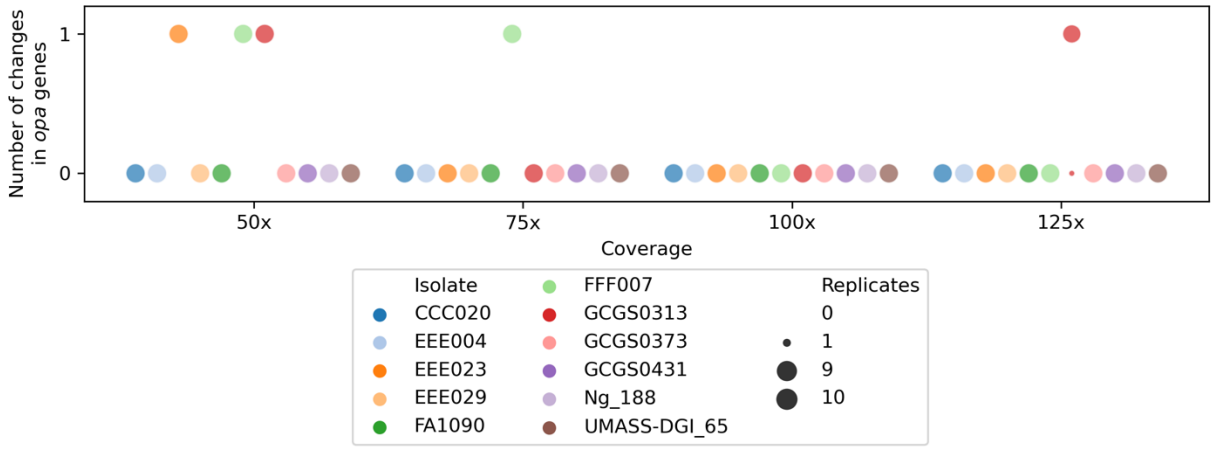

Figure S 2: More extensive comparison of *opa* sequences in Autocycler assemblies across 11 diverse isolates at 4 read coverage levels. The number of changes in *opa* genes at 4 read coverage levels using Autocycler. For each isolate, the reads were randomly subsampled 10 times at each read coverage (replicates) and an assembly was created with the subsampled reads using Autocycler. The size of the point indicates the number of replicates. The changes at 50x coverage include one SNP in two separate genomes and one undetected *opa*, the change at 75x was multiple sequence differences in one genome, and the change at 125x coverage was one SNP in one genome.

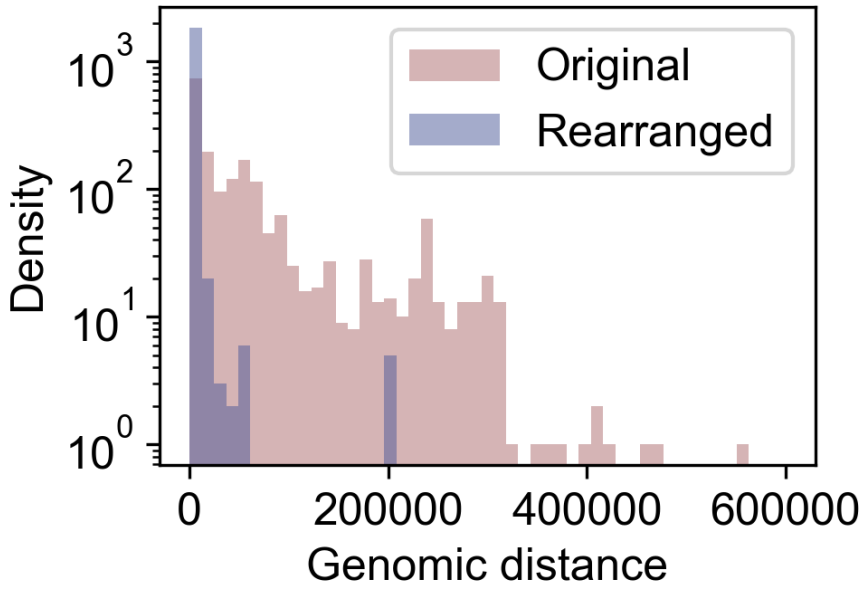

925

926 **Figure S 3**: **The distance between *opa* genes is higher in the original positions than after**
927 **accounting for genomic rearrangements**. The distances are calculated as the distance
928 between each *opa* in the reference genome FA1090 to the *opa* that is closest in genomic
929 position in all other isolates that had 11 *opa*.

930

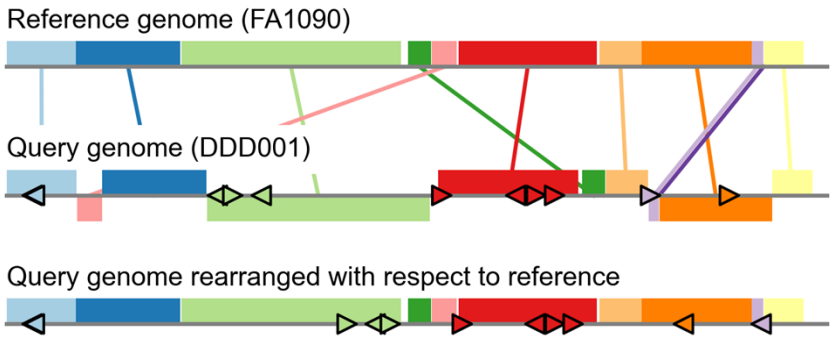

931

932 **Figure S 4:** Schematic of genomic rearrangement procedure (see Methods). The shaded
933 colored regions are the locally collinear blocks (LCBs). The LCBs that appear above the gray
934 line are on the forward strand and those that appear below the gray line are on the reverse

strand. A triangle pointing to the right indicates an *opa* gene on the forward strand and a triangle pointing to the left indicates an *opa* gene on the reverse strand.

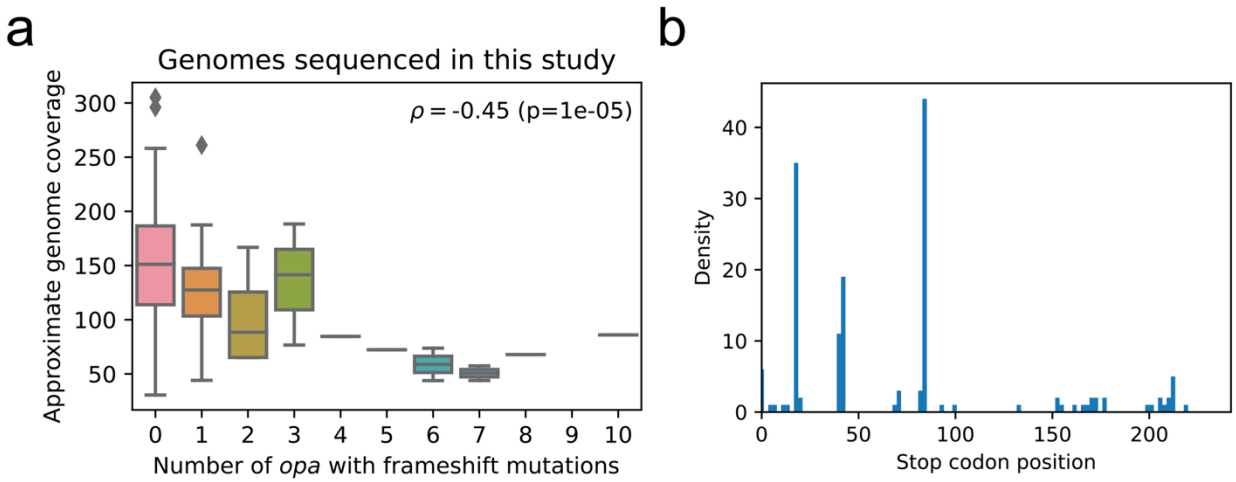

Figure S 5: A subset of *opa* genes exhibit frameshift mutations after coding repeats leading to a premature stop codon. (a) The approximate genome sequencing coverage and number of *opa* in the genome with frameshift mutations downstream of the coding repeats. (b) The locations of the stop codons in the *opa* genes with frameshift mutations downstream of the coding repeats. The maximum value of the x-axis is set at the average length of *opa* amino acid sequences.

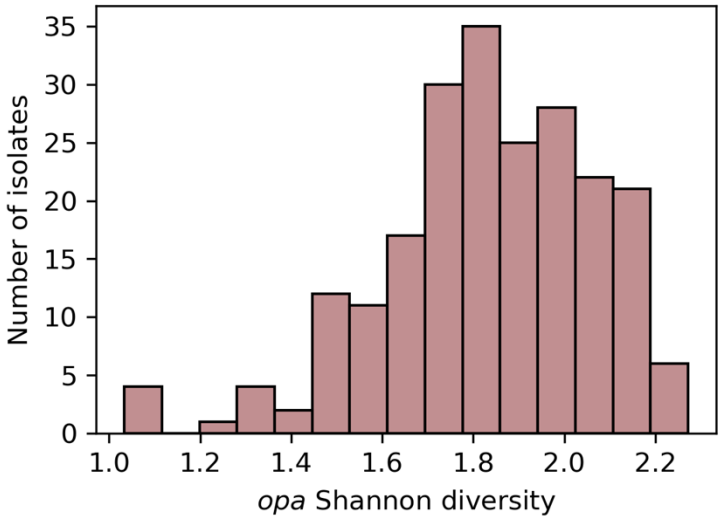

944

945 **Figure S 6: Shannon diversity of *opa* types within isolates**.

946

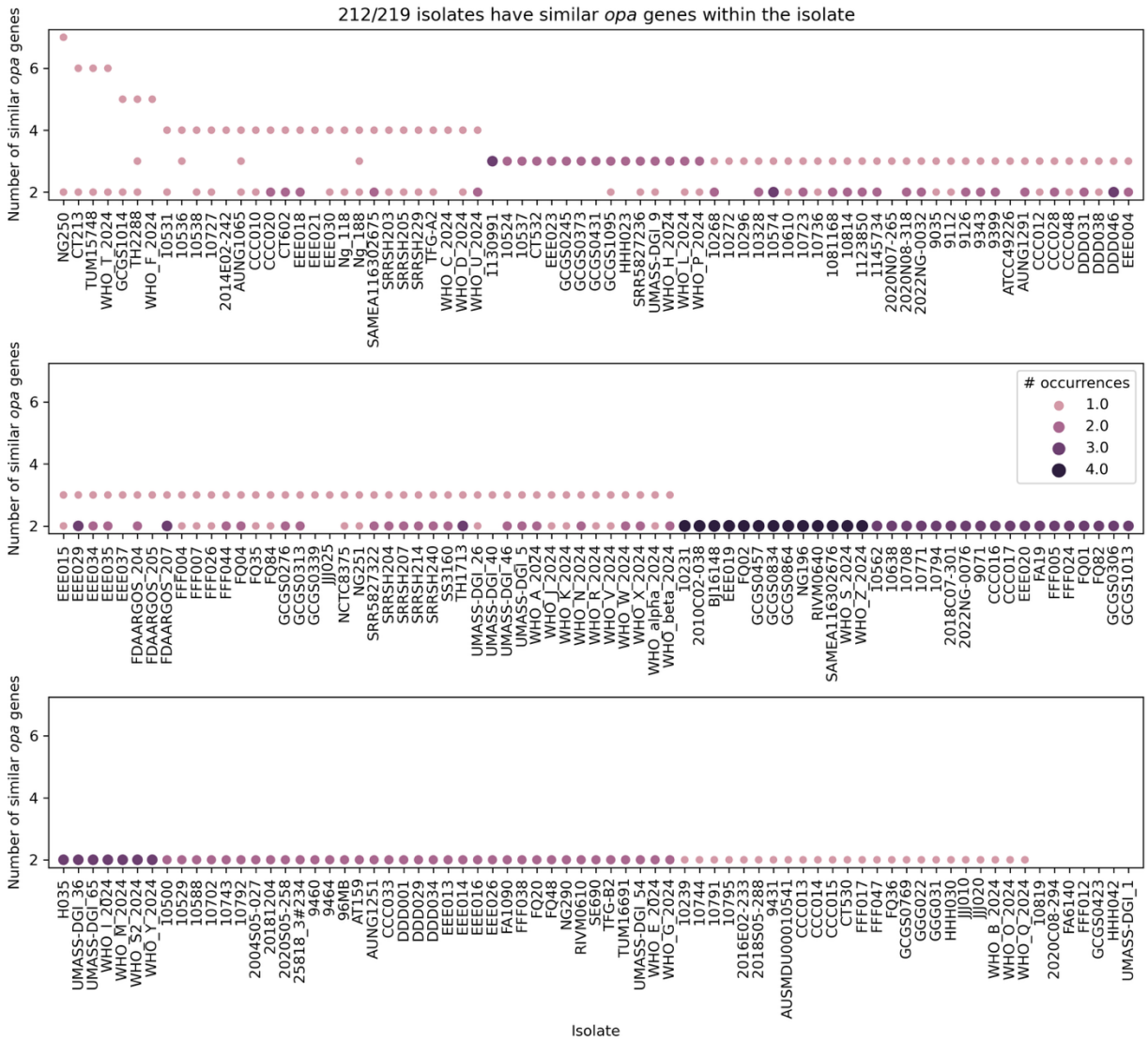

Figure S 7: **Genomes exhibit distinct patterns of similar *opa*s.** All isolates with complete genomes are shown on the x-axis. The points indicate groups of *opa* genes in the same isolate with >95% amino acid sequence identity. The y-axis shows the number of similar *opa* genes in each group. The size and color of the point indicate the number of distinct groups of each size in the genome. The x-axis is sorted first by the maximum number of similar *opa* genes in any group and then by the maximum number of groups. The plot is split into three rows for readability.

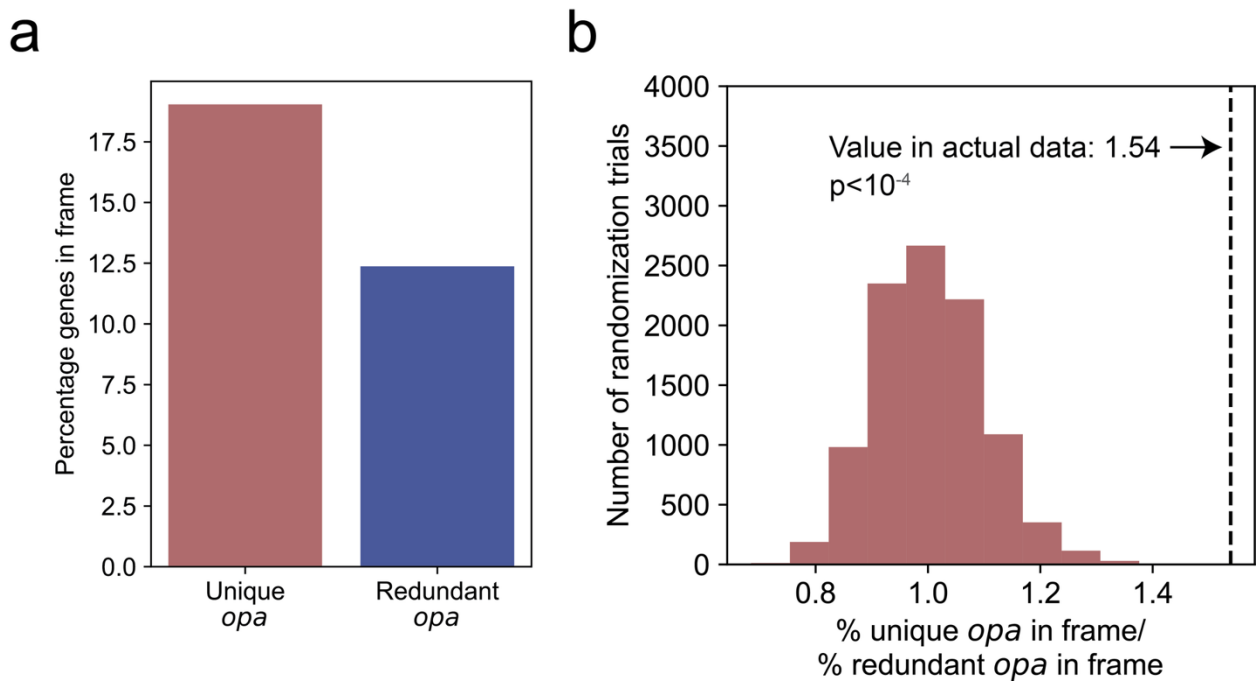

Figure S 8: The *opa* that are unique in an isolate are more likely to be in frame than the *opa* that are redundant. (a) The percentage of *opa* that are in frame for *opa* that are unique within an isolate (<95% amino acid similarity) or redundant within an isolate (≥95% amino acid similarity). (b) The ratio of the percentage of unique *opa* in frame to the percentage of redundant *opa* in frame for 10^4 randomizations of the data. The randomization procedure permuted which *opa* are labeled redundant, keeping the same total number of redundant *opa* across all isolates. Zero randomizations gave ratios as high as in the actual data (ratio of 1.54, indicated by the vertical dashed black line) yielding a p-value of less than 10^{-4}.

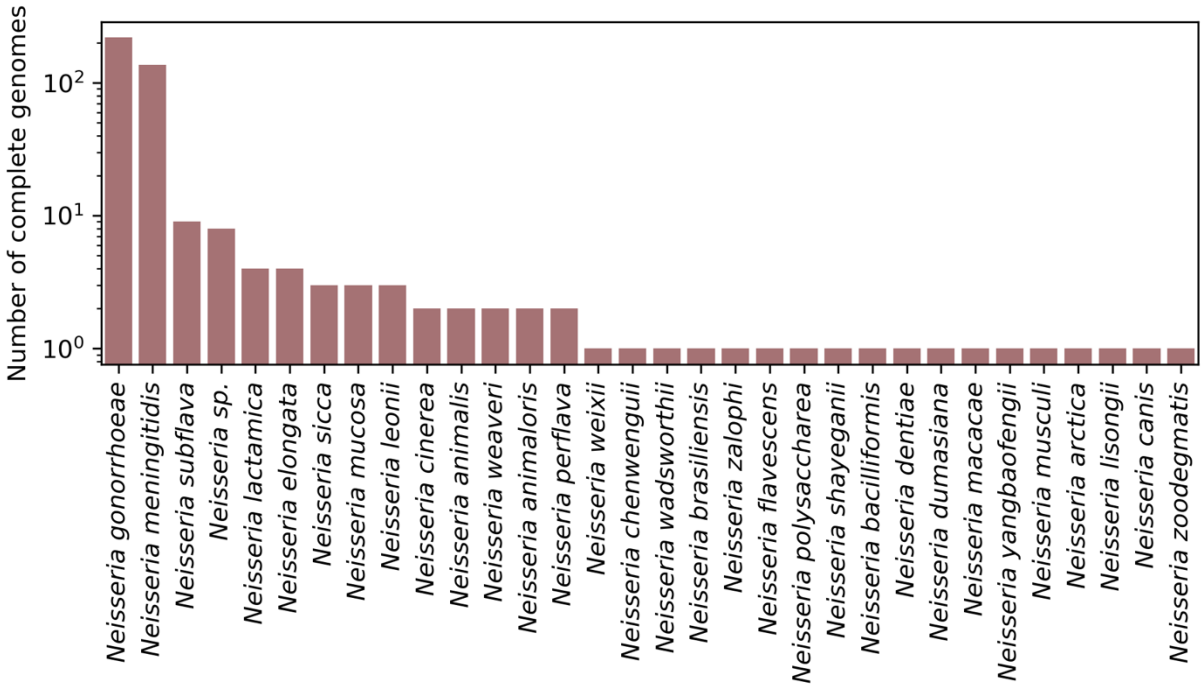

Figure S 9. The number of publicly available complete genomes by species from the *Neisseria* genus.

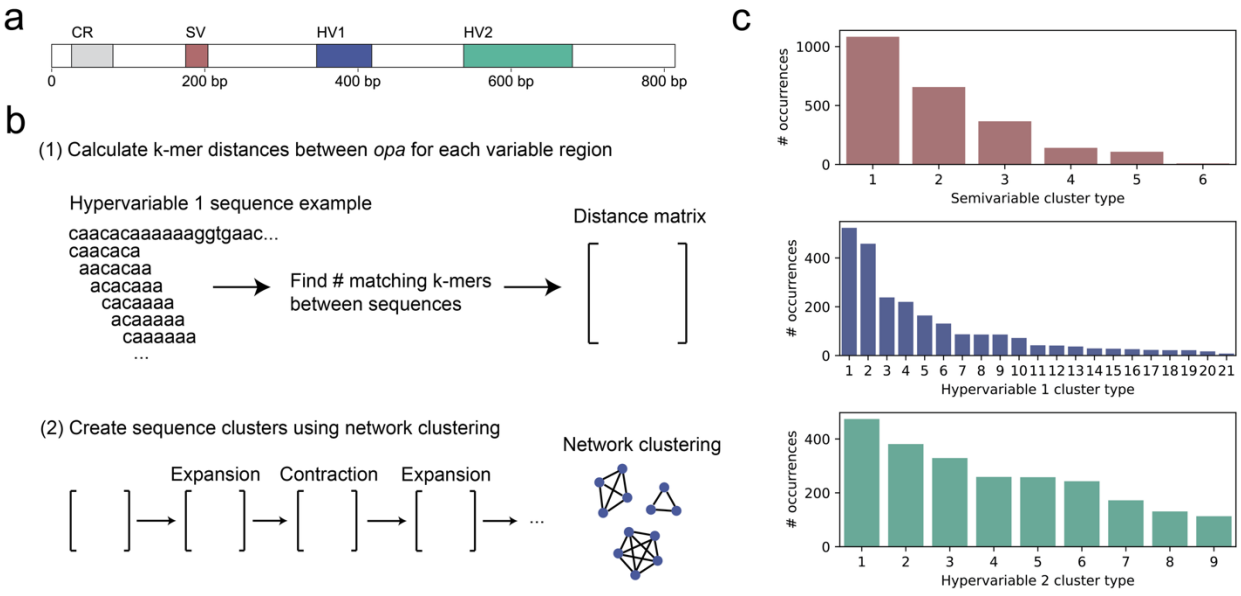

Figure S 10: Network-based clustering approach for semivariable and hypervariable *opa* sequences. (a) Schematic of the *opa* gene. The exact length and locations of the gene features varies across *opa* genes; depicted here is FA1090 *opa1*. CR: coding repeat, SV: semivariable region, HV1: hypervariable 1 region, HV2: hypervariable 2 region. (b) Summary of the approach to clustering variable region sequences. For each variable region (semivariable, hypervariable 1, and hypervariable 2), we calculated the k-mer distances between all sequences using MASH, setting k such that the probability of finding a random k-mer in each sequence is 0.01. We performed successive rounds of inflation (expansion and contraction) on the distance matrix, which amplifies high values of the matrix and suppresses low values of the matrix. We chose the lowest inflation parameter that gave a stable clustering. (c) The distribution of the cluster types for the sequences in each variable region.

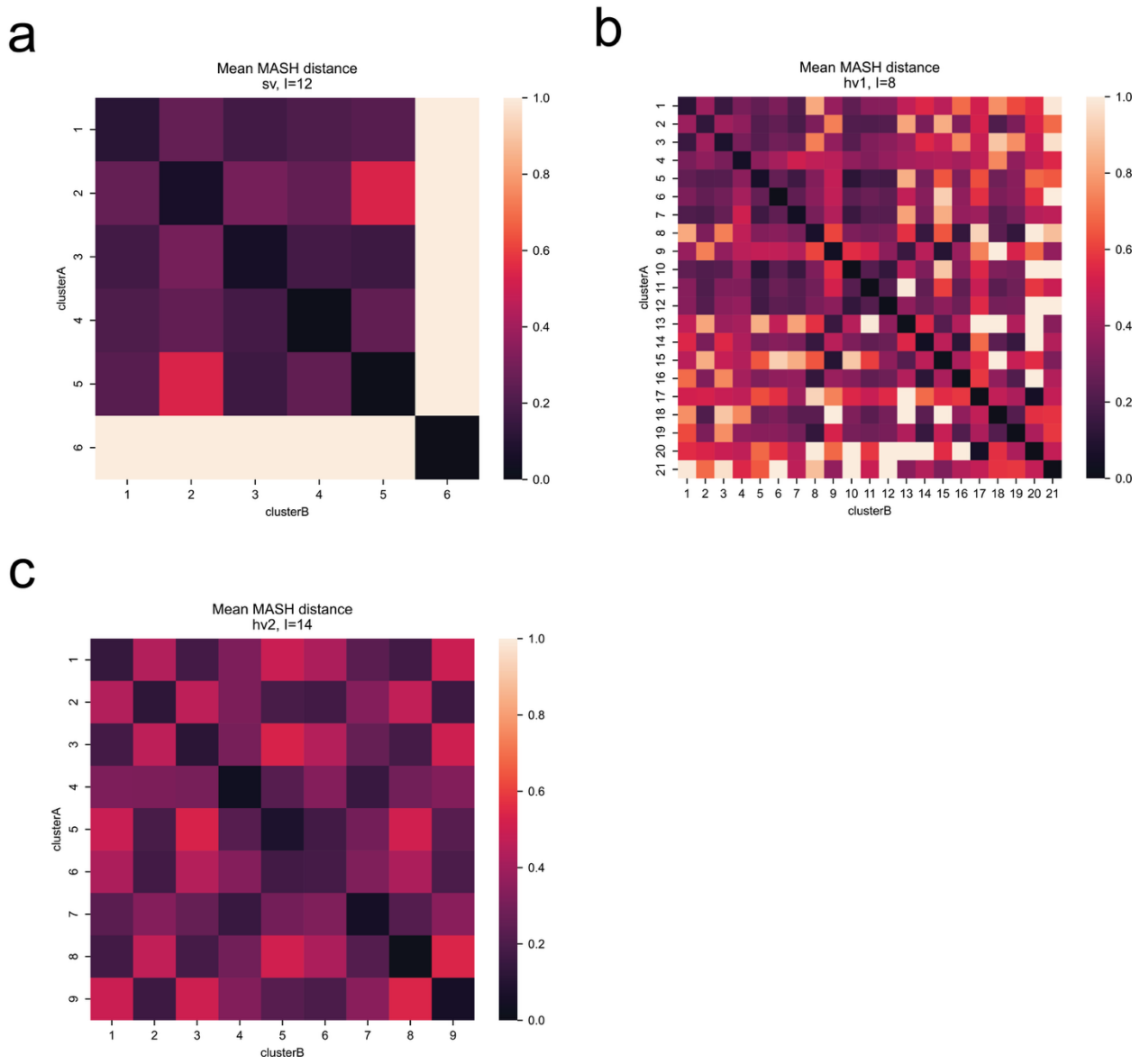

Figure S 11: Sequences generally are more similar within clusters than between clusters and clusters have distinct sequence motifs. The mean nucleotide distance between pairs of sequences in the same and different clusters in the semivariable (a), hypervariable 1 (b), and hypervariable 2 (c) regions.

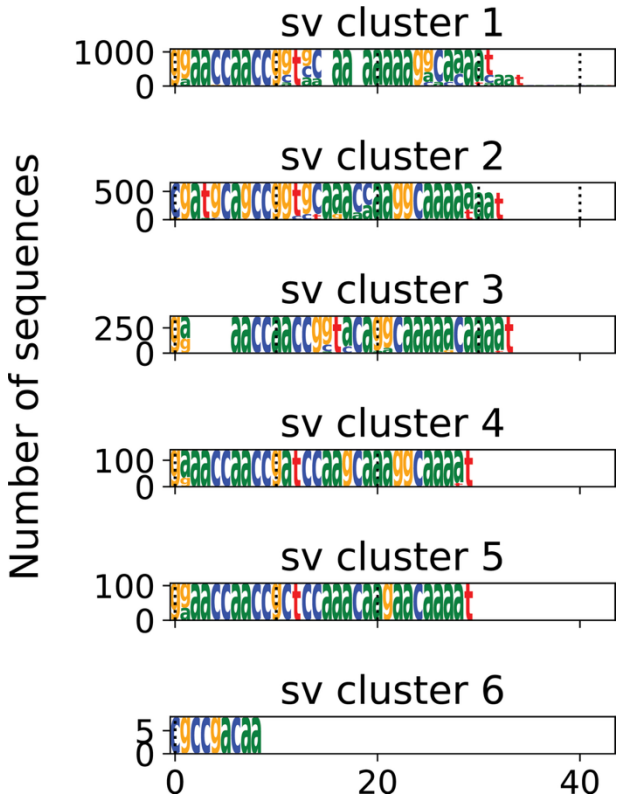

Figure S 12: The sequence logos for each cluster of the semivariable sequences. The nucleotide sequences were aligned using MAFFT in each cluster. The height of the nucleotides represents the number of sequences with each nucleotide.

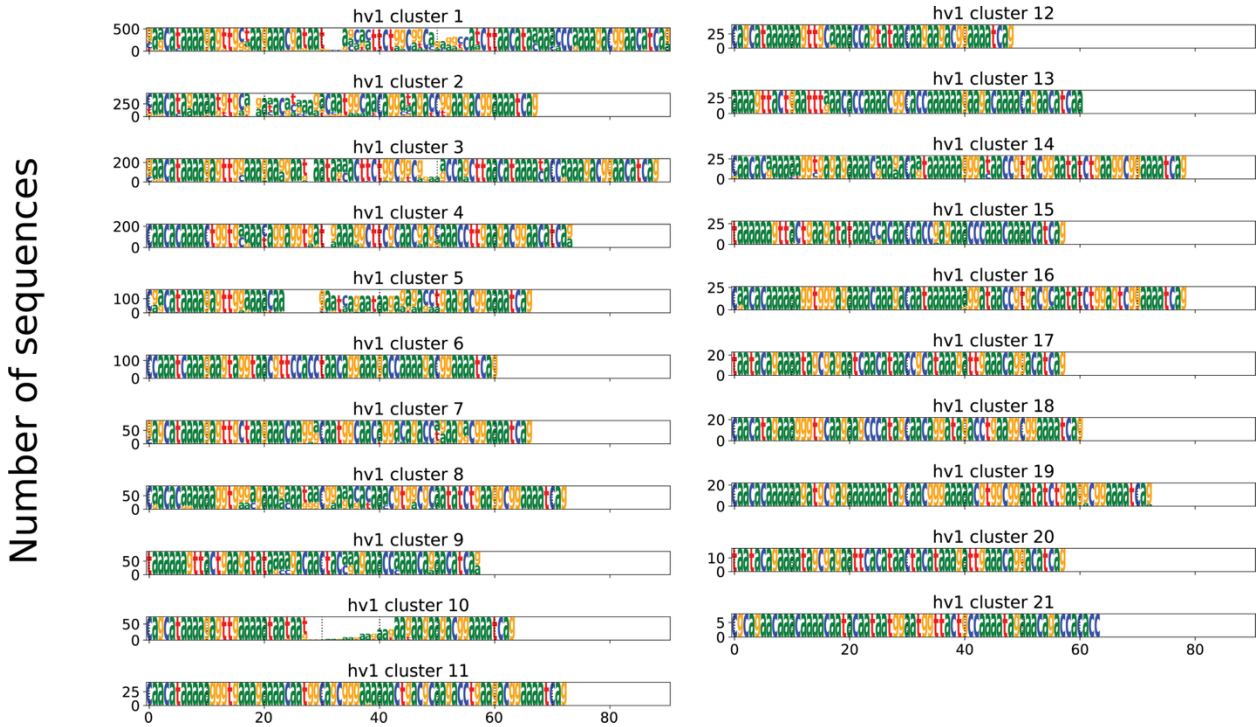

Figure S 13: The sequence logos for each cluster of the hypervariable 1 sequences. The nucleotide sequences were aligned using MAFFT in each cluster. The height of the nucleotides represents the number of sequences with each nucleotide.

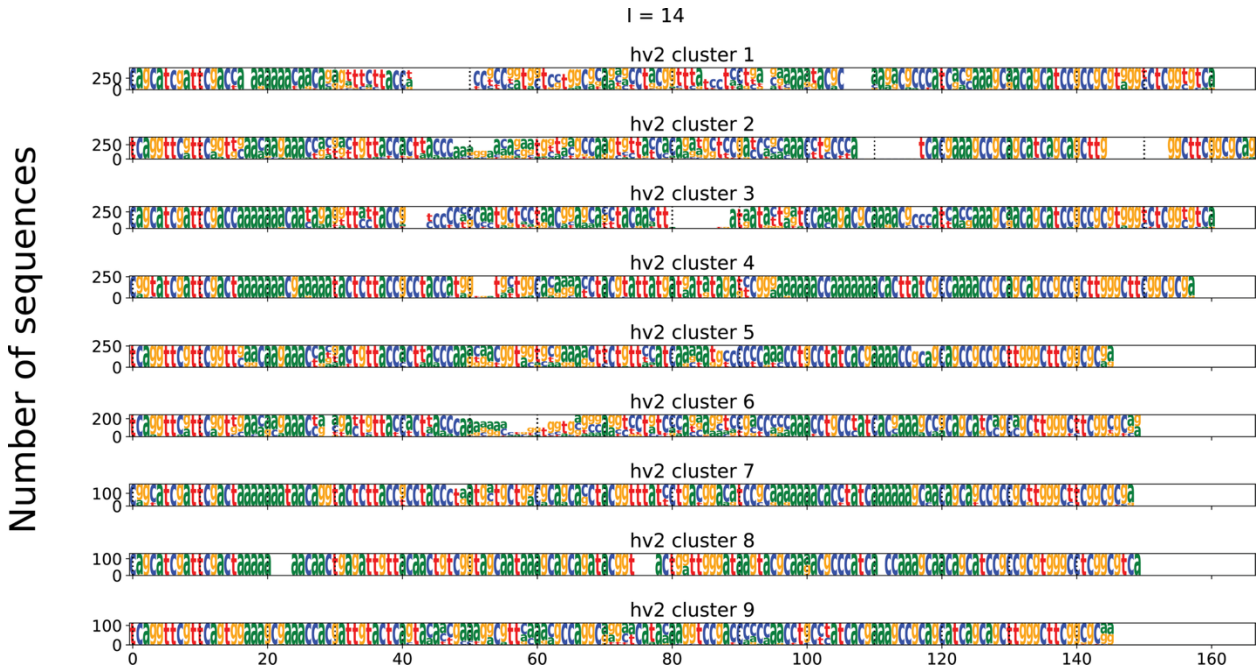

Figure S 14: The sequence logos for each cluster of the hypervariable 2 sequences. The nucleotide sequences were aligned using MAFFT in each cluster. The height of the nucleotides represents the number of sequences with each nucleotide.

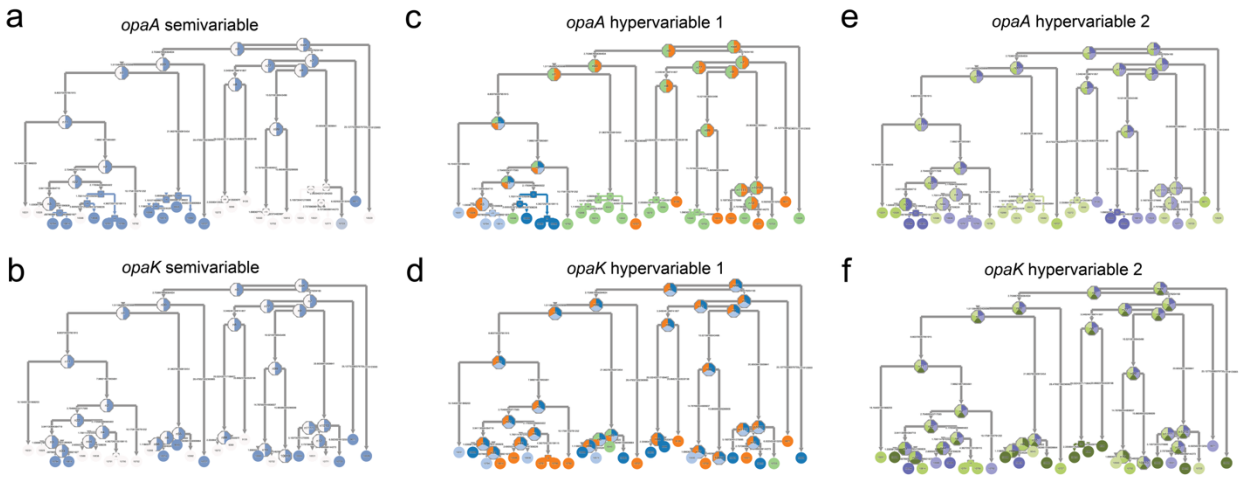

Figure S 15: *opaA* and *opaK* have similar cluster types that change at different rates. The dated phylogeny of the subtree shown in **Figure 6b** annotated with the cluster types for the

1009 semivariable (a-b), hypervariable 1 (c-d), and hypervariable 2 (e-f) regions shown as colored
1010 circles for *opaA* (a, c, e) and *opaK* (b, d, f). The colors are comparable within each sequence
1011 region across loci (e.g., the same color scheme is used for the semivariable region of both *opaA*
1012 and *opaK*) but not between sequence regions. The colored circle annotations at the tips
1013 represent the cluster types of the isolates, and the colored circle annotations in the internal
1014 nodes represent the inferred ancestral state by PastML. The cluster types that are present in
1015 *opaA* and *opaK* are similar, but more closely related isolates have more similar cluster types in
1016 *opaA* compared to *opaK*.

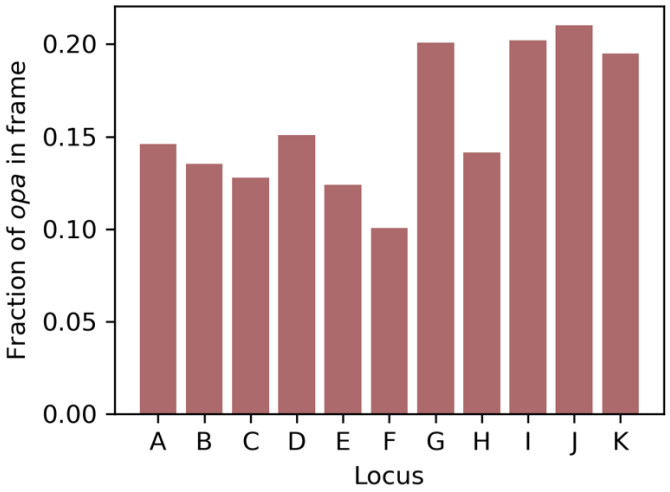

1017

1018 **Figure S 16: No significant differences in fraction in of *opa* in frame by locus.** One-sided
1019 proportions *Z*-tests with a Bonferroni multiple hypothesis correction comparing the fraction of
1020 *opa* in frame at each locus (1) to the total fraction of *opa* in frame across all loci and (2) to the
1021 fraction of *opaK* alleles that are in frame are not significant.

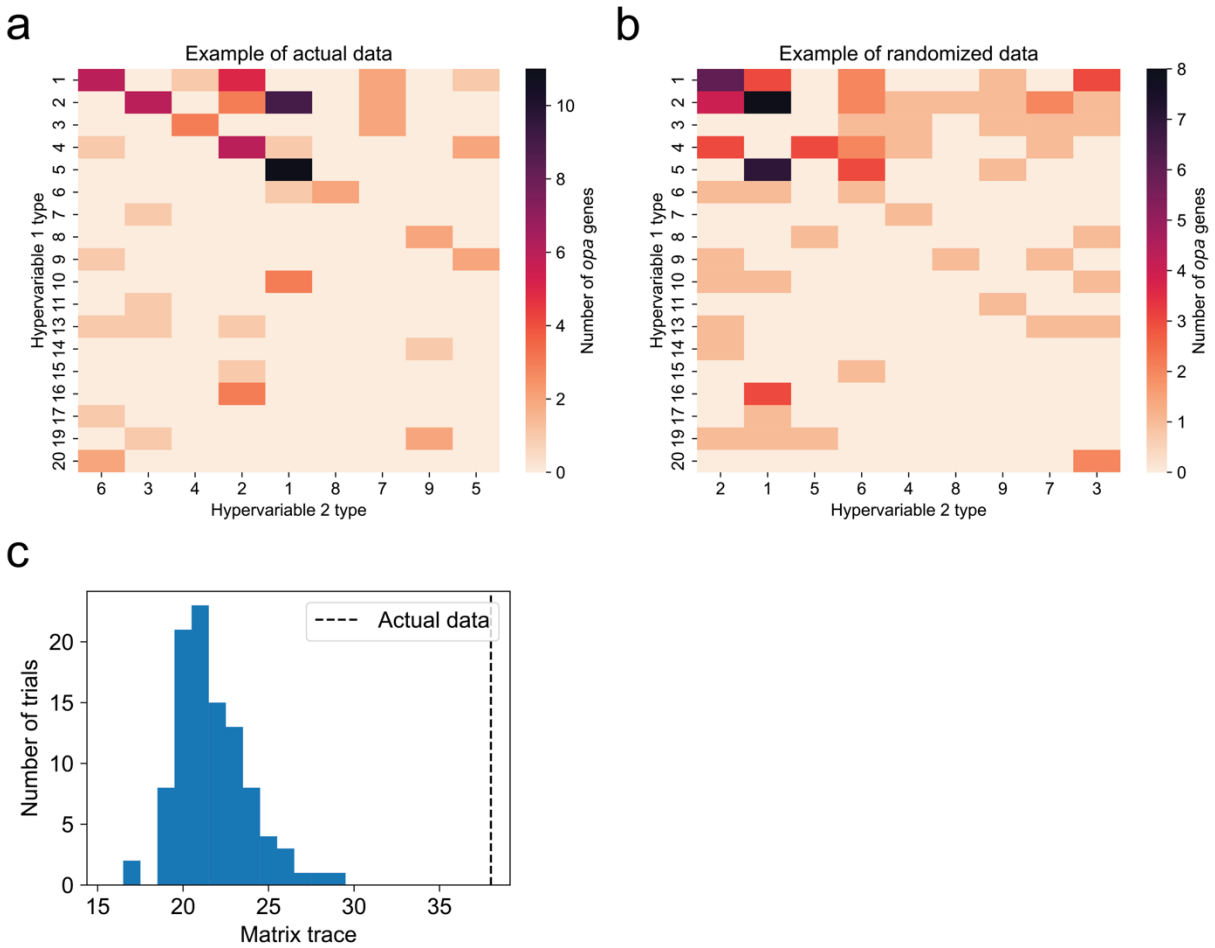

Figure S 17: Non-random association of hypervariable 1 and hypervariable 2 allele types in *opa* genes, as shown for one representative random subset of 1 isolate per BAPS cluster. (a) The number of each combination of hypervariable 1 and hypervariable 2 types in *opa* alleles after accounting for isolate sampling and population structure. The columns of the matrix were rearranged to give the largest matrix trace (padding with columns of all zeros to make a square matrix). (b) The same data representation in (a) but after randomizing the assignment of hypervariable 2 types across the *opa* alleles. (c) The distribution of the maximum sum of the diagonal matrix elements (allowing for column rearrangements) in 100 randomizations of the hypervariable 2 type (blue histogram) compared to the actual data (black dashed line).

1034

1035 **Supplementary Information**

1036

1037 Supplementary Methods

1038

1039 *Short-read sequencing*

1040 Short-read sequencing for EEE029 was performed in Bristow, Mortimer, et al. [68] and short-
1041 read sequencing of UMASS-DGI_65 was performed using the same method. Briefly, DNA was
1042 extracted from bacterial cells grown overnight on GCB-K plates at 37°C with 5% carbon dioxide
1043 using the Invitrogen PureLink Genomic DNA Mini Kit. Libraries were prepped and sequenced on
1044 the Illumina NextSeq 2000 sequencer at the Microbial Whole Genome Sequencing Center or
1045 the Bauer Core Facility at Harvard University.

1046

1047 *Comparison of long-read assembly and polishing methods*

1048 To develop a pipeline for assembling complete genomes to minimize errors in the *opa* genes,
1049 we used the following assembly and polishing approaches using the filtered long-reads from
1050 Oxford Nanopore (see Methods) and short reads generated by Illumina NextSeq: Flye v2.9.5
1051 [27], Medaka v2.0.1 (https://github.com/nanoporetech/medaka), Polypolish v0.6.0 [69], Pypolca
1052 v0.3.1 [69], and Autocycler v0.2.1 [25]. We tested the following workflows:

1053 1. Long-read only assembly with Flye.
1054 2. Long-read only assembly with Flye → long-read polishing with Medaka
1055 3. Long-read only assembly with Flye → long-read polishing with Medaka → short-read
1056 polishing with Polypolish default
1057 4. Long-read only assembly with Flye → long-read polishing with Medaka → short-read
1058 polishing with Polypolish default followed by short-read polishing with Pypolca careful
1059 5. Long-read only assembly with Autocycler

1060 6. Long-read only assembly with Autocycler → short-read polishing with Polypolish default
1061 7. Long-read only assembly with Autocycler → short-read polishing with Polypolish default
1062 → short-read polishing with Pypolca careful

1063 We used the genomes UMASS-DGI_65 and EEE029 which had sequencing depth of around
1064 140x. To test how sequencing depth would affect the *opa* sequence accuracy, we randomly
1065 subsampled the reads using the seqtk package v1.4 (https://github.com/lh3/seqtk) to 15% (21x),
1066 30% (42x), and 60% (84x), and compared to the results including 100% of the reads (140x). For
1067 each read subset, we assembled the genome using the approaches above and identified the
1068 *opa* sequences as described in the Methods. We aligned the resulting *opa* sequences using
1069 MAFFT v7.520 [35] with the default parameters.
1070

1071 *More extensive testing of Autocycler with different read depth across diverse isolates*

1072 We selected 11 phylogenetically diverse isolates with at least 125x coverage using Treemmer
1073 v0.3 [70]. We created 10 random read subsets using the seqtk package at 50x, 75x, 100x, and
1074 125x coverage. We assembled the genomes using the following approaches. We assembled
1075 the genomes (using long reads only) using Autocycler and followed the approach above to
1076 compare *opa* sequences.
1077

1078 *Algorithm to search for* opa *genes in the complete genomes*

1079 We wrote a custom python script to identify *opa* genes. First, we searched for 3 to 100 tandem
1080 repeats of the CTCTT pentanucleotide with at most 2 substitutions across the entire sequence,
1081 which we will refer to as the coding repeats (CR), similar to the approach used in Bilek et al.
1082 [21]. We then searched for the unique conserved sequence near the stop codon
1083 (TGCGCTACCGCTTCTGAT) with at most 2 substitutions, which we will refer to as the term
1084 sequence. Pairs of CR and term sequences were matched if they were separated by less than
1085 1200 bp in the genome. For term sequences that were unpaired, a more lenient search was

1086 performed for the upstream CR where we allowed up to 1 error for each CR unit (substitution,
1087 insertion, or deletion) to catch CR units that contained mutations. If there was still not a
1088 matching CR found, it could have been that the *opa* did not have a CR; in this case, we looked
1089 for the sequence found directly upstream of the CR consisting of a poly-A sequence of length 5-
1090 7 followed by CCTT and allowed one error (substitution, insertion, or deletion).
1091
1092 The start codon (ATG) was identified in the 50 bp upstream of the start of the CR sequence and
1093 the stop codon (TGA) was contained in the term sequence. Occasionally, the beginning and end
1094 of the CR region was not defined precisely with the above procedure due to errors in the CR
1095 (substitution, insertion, or deletion). Thus, the start of the CR was made more precise by finding
1096 the upstream sequence (see end of previous paragraph). If this sequence was not found, then
1097 the start of CR from earlier was used. Similarly, the end of the CR was made more precise by
1098 searching for the downstream sequence, which is CCG, allowing for the first C to be optional
1099 and 1 additional error.
1100
1101
1102 *Calculation of the randomness of hypervariable 1 and hypervariable 2 allele types*
1103
1104 We dropped duplicate *opa* genes in the same genome as determined by having the same
1105 semivariable, hypervariable 1, and hypervariable 2 cluster type combinations to remove the
1106 effect of recent gene conversion events that have not yet had the time to be subject to selection.
1107
1108 We accounted for isolate sampling and *N. gonorrhoeae* population structure by partitioning the
1109 recombination-corrected phylogeny of complete genomes using fastbaps v1.0.8 [71] with the
1110 BAPS prior. We randomly selected 1 isolate from each BAPS cluster.
1111

1112 We determined the number of times each hypervariable 1 and hypervariable 2 cluster types
1113 appeared together in all *opa* genes in the subsampled isolates and created an association
1114 matrix where the rows were hypervariable 1 types, the columns were hypervariable 2 types, and
1115 the element values were the number of times each combination appeared. Because the number
1116 of hypervariable 1 and hypervariable 2 types were unequal, we padded columns with zeros to
1117 give a square matrix. We determined the degree of association by rearranging the columns of
1118 the association matrix to maximize the sum of diagonal entries using the Munkres algorithm
1119 (https://github.com/bmc/munkres?tab=readme-ov-file, v1.1.4). To determine whether the
1120 observed data could be random, we randomized the hypervariable 2 cluster types across the
1121 *opa* genes 100 times. We compared the maximum sum of diagonal elements from the observed
1122 data and the randomized data. We then repeated this process by performing 99 random
1123 subsamples of the isolates in each BAPS cluster.
1124
1125 *Quantification of frameshift mutations downstream of the coding repeats leading to a premature*
1126 *stop codon*
1127 We identified all *opa* amino acid sequences that had a premature stop codon after the end of
1128 the coding repeat sequence. The approximate genome coverage was calculated as the number
1129 of input read bases divided by the number of consensus assembly bases. To identify the
1130 location of the frameshift mutations, the nucleotide sequences were aligned with MAFFT v7.520
1131 [35] with the default parameters and visualized in Jalview v2.11.4.1 [36].
1132
1133 Comparison of long-read assembly and polishing methods
1134 We first compared multiple assembly and polishing approaches, including Flye, Medaka,
1135 Polypolish, Pypolca, and Autocycler at 4 read depths (21x, 42x, 84x, and 140x) for two
1136 genomically diverse isolates. The *opa* sequences were identical across assemblies except for 1
1137 SNP in UMASS-DGI_65 *opa7* and a 1 base insertion in EEE029 *opa11*, both of which occurred

1138 in methods 1 (long-read assembly with Flye) and 2 (long-read assembly with Flye followed by
1139 long-read polishing with Medaka) for a read depth of 21x (**Figure S 1**). This analysis suggested
1140 Autocycler was the best performing assembly method and that polishing the Autocycler
1141 assemblies with short reads did not affect the *opa* sequences. However, because we only
1142 tested 2 genomes, we wanted to expand the analysis to include more isolates that are
1143 representative of *N. gonorrhoeae* diversity and to subset the reads to test lower read depths
1144 more systemically.
1145
1146 In our more extensive testing of Autocycler using 11 diverse isolates and 4 read depths (50x,
1147 75x, 100x, and 125x) the *opa* sequences were identical across assemblies except for the
1148 following differences (always compared to 125x coverage assembly) (**Figure S 2**):
1149 - EEE023 *opa4* had 1 SNP in 10/10 assemblies with 50x coverage.
1150 - FFF007 *opa11* was not detected in 10/10 assemblies with 50x coverage due to a
1151 missing stop codon and had multiple sequence differences in 10/10 assemblies with 75x
1152 coverage.
1153 - GCGS0313 *opa1* had a 1 base deletion in 9/10 assemblies with 125x coverage
1154 - GCGS0313 *opa5* had 1 SNP in 10/10 assemblies with 50x coverage
1155
1156 Despite these changes in a small number of *opa* sequences, we concluded that most *opa*
1157 sequences were identical across read depths and that Autocycler assemblies were good
1158 enough for our purposes of looking at diversity and evolution across a large set of *opa* genes.
1159
1160 **Supplementary Tables**
1161 **Table S1. Publicly available complete genomes.**
1162 **Table S2. Complete genomes sequenced in this study.**

1163 **Table S3. References for publicly available *N. gonorrhoeae* short-read sequencing data**

1164 **meeting quality control thresholds for selection of representative draft genomes.**

1165 **Table S4. Representative *N. gonorrhoeae* draft genomes.**

1166 **Table S5. Publicly available *Neisseria* species complete genomes.**

1167